UC Riverside
UC Riverside Electronic Theses and Dissertations

Title
Growth of Atomic Hexagonal Boron Nitride Layers and Graphene/Hexagonal Boron Nitride Heterostructures by Molecular Beam Epitaxy

Permalink
https://escholarship.org/uc/item/0dp41524

Author
Xu, Zhongguang

Publication Date
2016

Peer reviewed|Thesis/dissertation

eScholarship.org Powered by the California Digital Library
University of California

UNIVERSITY OF CALIFORNIA
RIVERSIDE

Growth of Atomic Hexagonal Boron Nitride Layers and Graphene/Hexagonal Boron Nitride Heterostructures by Molecular Beam Epitaxy

A Dissertation submitted in partial satisfaction
of the requirements for the degree of

Doctor of Philosophy

in

Electrical Engineering

by

Zhongguang Xu

December 2016

Dissertation Committee:
Dr. Jianlin Liu, Chairperson
Dr. Elaine Haberer
Dr. Gang Chen

Copyright by
Zhongguang Xu
2016

The Dissertation of Zhongguang Xu is approved:

____

____

____
Committee Chairperson

University of California, Riverside

ACKNOWLEDGEMENTS

First of all, I would give my appreciation to my advisor Prof. Jianlin Liu. I am truly thankful to him for letting me have this chance to study in his group. And his guidance, inspiration and patience brought me into the way toward high-class research during the past four years. Although I met so many problems, he was always helpful and showed the knowledge and skills, which trained me the basis experimental skills and scientific research mind. I really learned a lot from the way he is thinking and he is doing, which will definitely benefit my future life. I would express my deepest gratitude to him at this moment.

I would also like to thank my final dissertation defense committee members, Dr. Chen and Dr. Haberer, for their time, insightful questions and helpful comments. I want to thank my labmates Dr. Zheng Zuo, Dr. Jian Huang, Dr. Monzur Morshed, Mr. Mohammad Suja, Ms. Sunayna Bashar, Mr. Alireza Khanaki, Ms. Renjing Zheng, Mr. Hao Tian, Mr. Wenhao Shi and others who gave me help during my PhD research and study.

Finally, I would like to give my appreciation to my wife and my parents. Their encouragement, company and support make this dissertation to come true. I will treasure and share all the moments with you in my life. Thank you for everything.

Previously Published Material Acknowlegment

1) The results in Chapter 2 were published in "Z. Zuo, Z. Xu (co-first author), R. Zheng, A. Khanaki, J. Zheng, and J. Liu, Sci. Rep., 5, 14760 (2015)". (http://www.nature.com/articles/srep14760)

2) The results in Chapter 3 were published in "Z. Xu, A. Khanaki, H. Tian, R. Zheng, J. Zheng, and J. Liu, Appl. Phys. Lett. 109, 043110 (2016)". (http://scitation.aip.org/content/aip/journal/apl/109/4/10.1063/1.4960165)

3) The results in Chapter 4 were published in "Z. Xu, R. Zheng, A. Khanaki, Z. Zuo, and J. Liu, Appl. Phys. Lett. 207, 213103(2015)". (http://scitation.aip.org/content/aip/journal/apl/107/21/10.1063/1.4936378)

4) The main results in Chapter 5 were submitted to Scientific Report on August 5th (2016) .

ABSTRACT OF THE DISSERTATION

Growth of Atomic Hexagonal Boron Nitride Layers and Graphene/Hexagonal Boron Nitride Heterostructures by Molecular Beam Epitaxy

by

Zhongguang Xu

Doctor of Philosophy, Graduate Program in Electrical Engineering
University of California, Riverside, December 2016
Dr. Jianlin Liu, Chairperson

Graphene, as a famous Van der Waals material, has attracted intensive attention from research group and industry all over the world after 2004, while hexagonal boron nitride (h-BN), as an excellent two-dimensional (2D) dielectric layer, has been studied intensively mainly for its compatibility with graphene and other 2D materials. To realize the technological potential of 2D system, it is essential to synthesize large-area, high-quality 2D thin films through a scalable and controllable method in order to investigate novel phenomenon in fundamental physics and promising device applications. In this thesis, the growth of graphene, h-BN and their vertical and lateral heterostructures by molecular beam epitaxy (MBE) is mainly discussed. In addition, the growth mechanism, fundamental physics and possible applications are also studied.

In-situ epitaxial growth of graphene/h-BN heterostructures on cobalt (Co) film substrate was achieved by using plasma-assisted MBE in Chapter 2. We demonstrated a solution for direct fabricating graphene/h-BN vertical stacking structures. Various

characterizations, such as Raman spectroscopy, scanning electron microscopy (SEM), X-ray photoelectron spectroscopy (XPS) and transmission electron microscopy (TEM), were carried out to confirm and evaluate the heterostructures. Wafer-scale heterostructures consisting of single-layer/bilayer graphene and multilayer h-BN were achieved. The mismatch angle between graphene and h-BN is below 1°. Chapter 3 studied the growth of graphene/h-BN heterostructures on Co foil substrate by plasma-assisted MBE. It is found that the coverage of h-BN layers on the epitaxial thin graphite layer is growth-time dependent. Large-area, uniform-quality h-BN film was successfully deposited on thin graphite layer. Based on the as-grown h-BN (5-6 nm)/G (26-27 nm) heterostructure, without using any transferring process, we fabricated capacitor devices with Co(foil)/G/h-BN/Co(contact) configuration to evaluate the dielectric properties of h-BN film. The measured breakdown electric field showed a high value of 2.5-3.2 MV/cm. Both I-V and C-V characteristics indicated that the epitaxial h-BN film is of good insulating nature.

Following with the lateral growth of graphene on in situ epitaxial h-BN flakes by plasma-assisted MBE is discussed in Chapter 4. Single-crystal h-BN domains were grown on Co film substrates at a substrate temperature of 850~900 ^{o}C using plasma-assisted MBE. Three-point star shape h-BN domains were observed by SEM, and confirmed by Raman and XPS. The h-BN on Co template was used for in situ growth of multilayer graphene, leading to an h-BN/graphene heterostructure. Carbon atoms preferentially nucleate on Co substrate and edges of h-BN and then grow laterally to form continuous graphene. Further introduction of carbon atoms results in layer-by-layer

growth of graphene on graphene and lateral growth of graphene on h-BN until it may cover entire h-BN flakes.

The final part (Chapter 5) is related to the growth of large-area and multi-layer h-BN film on polished Co foils by plasma-assisted MBE. The coverage of h-BN layers can be readily controlled by growth time under appropriate growth conditions. A large-area, multi-layer h-BN film is confirmed by various characterizations. Dielectric property of as-grown h-BN film is evaluated by characterization of Co(foil)/h-BN/Co(contact) capacitor devices. Breakdown electric field is in the range of 3.0-3.3 MV/cm, which indicates that the epitaxial h-BN film has good insulating characteristics. In addition, the effect of substrate morphology on h-BN growth is discussed regarding different domain density, lateral size, and thickness of the h-BN films grown on unpolished and polished Co foils.

Table of Contents

Acknowledgements iv

Abstract vi

Table of Contents ix

List of Figures xi

List of Tables xv

Chapter 1: Introduction 1

1.1 Graphene.. 1

1.2 Hexagonal Boron Nitride 3

1.2.1 Exfoliation.. 4

1.2.2 CVD.. 6

1.2.3 PVD 7

1.3 Heterostructures based on graphene and h-BN 8

1.4 Motivation of 2D materials growth by molecular beam epitaxy 10

1.5 Chapter arrangement 11

Reference.. 14

Chapter 2: In-situ epitaxial growth of graphene/h-BN heterostructures on Co film substrate using plasma-assisted MBE.. 21

2.1 Introduction 21

2.2 Material growth, device fabrication and characterization method.. 22

2.3 Results and discussion.. 24

2.4 Summary.. 32

Reference.. 33

Chapter 3: Growth of graphene/h-BN heterostructures on Co foil substrate by plasma-assisted MBE.. 37

3.1 Introduction 37

3.2 Material growth, device fabrication and characterization method.. 39

3.3 Results and discussions 41

3.4 Summary.. 51

Reference..52
Chapter 4: Lateral growth of graphene on in situ epitaxial h-BN flakes by plasma-assisted MBE..57
4.1 Introduction..57
4.2 Materials growth and characterization..58
4.3 Results and discussions..60
4.4 Summary..66
References..67
Chapter 5: Growth of large-area and multi-layer hexagonal boron nitride film on polished Co foils by plasma-assisted MBE..71
5.1 Introduction..71
5.2 Sample preparation and characterization..73
5.3 Results and discussion..78
5.4 Summary..88
Chapter 6: Summary..95

List of Figures

Figure 1-1 Schematic of monolayer graphene. (Source: Wikipedia.org) (Page 2)

Figure 1-2 Schematic of hexagonal boron nitride layers. (Source: Wikipedia.org) (Page 3)

Figure 2-1 (a) Optical microscopy image of graphene/h-BN heterostructure sample (b) SEM image of graphene/h-BN heterostructure on cobalt substrate (Sample A). Inset is taken under the same condition with larger magnification, and it shows a large triangular h-BN flake of about 20 μm. The background is the rough substrate surface with packed Co grains resulted from heat treatment. (Page 25)

Figure 2-2 (a) and (b) are typical graphs with (a) showing both h-BN E_{2g} optical phonon peak at 1360 cm^{-1} and signature graphene G and 2D peaks at discrete locations, and (b) showing only graphene peaks across the entire surface. (Page 26)

Figure 2-3 (a) Optical microscopy image and SEM image (b) of graphene/h-BN sample with wafer-scale coverage (Sample B). (Page 27)

Figure 2-4 XPS spectra of graphene/h-BN heterostructure on Co substrate (Sample B). a) Survey spectrum, b) N1s peak, c) C1s peak, and d) B1s peak. B1s and N1s are at 190.6 eV, and 398.0 eV, respectively, indicating the existence of h-BN. C1s peak is at 284.5 eV, indicating the presence of graphene. (Page 28)

Figure 2-5 Raman spectrum of graphene/h-BN heterostructure (Sample B). Evident graphene G and 2D peaks are observed, with their intensity ratio indicating 1~2 layer graphene. The inset is enlarged spectrum in the 1300~1400 cm^{-1} region. Two peaks are resolved, relating to graphene D mode and E_{2g} optical phonon peak of h-BN, respectively. (Page 29)

Figure 2-6 (a) Plan-view TEM image of transferred graphene/h-BN heterostructure (Sample B). (b) SAED pattern of Sample B. Diffraction patterns with six-fold symmetry are observed. The inset is enlarged image of the red square area marked in (b). Two diffraction spots are observed, revealing the (100) plane distance of 2.13 Å and 2.06 Å, respectively. (c) Cross-sectional TEM image of Sample B. The thickness of the heterostructure is about 15 nm. (Page 30)

Figure 2-7 (a) Schematic of the transistor device, (b) an optical microscopy image of the transistor device. (c) I_D–V_G characteristics, and (d) I_D-V_D characteristics. (Page 31)

Figure 3-1 Schematic of the growth process of h-BN/G stacked heterostructures. (a) Cleaned Co foil substrate. (b) Layer-by-layer graphene structure grown on fresh Co foil surface. (c) Triangular h-BN domains grown on top of the graphene layers. (d) Connection of triangular h-BN domains to form the first continuous h-BN layer, followed by layer-by-layer growth of h-BN. (Page 41)

Figure 3-2 Photographs of (a) bare Co foil substrate and (b) as grown h-BN/G sample (Sample D). (Page 42)

Figure 3-3 SEM image of (a) the graphene (G) on Co foil (Sample A); and h-BN on G film at different h-BN layer growth time: (b) 300 s (Sample B), (c) 1200 s (Sample C),

and (d) 1800 s (Sample D). Insets in (b), (c) and (d) are magnified SEM images of local surface areas of these samples. Scale bars in (a-d) are 50 μm. Scale bars for insets in (b-d) are 20 μm. (Page 43)

Figure 3-4 (a) Raman spectra of as-grown graphene (Sample A) and h-BN/G heterostructure (Sample D). The G/2D peak ratio in both samples indicates the existence of multilayer graphene. Additional peak is observed besides G and 2D peaks for the h-BN/G sample at 1368 cm^{-1}, corresponding to the E_{2g} optical phonon mode of h-BN. (b) UV-Vis absorption spectrum of a transferred h-BN/G sample on sapphire. (c) α^2 as a function of photon energy. XPS spectra of (d) C1s, (e) N1s, and (f) B1s signals. (page 45)

Figure 3-5 (a) Optical microscopy and (b) AFM images of Co foil after high-temperature annealing in vacuum. (c) AFM image of as-grown film, (d) Optical microscopy, and (e-f) AFM images of transferred film of Sample D on SiO_2. (Page 45)

Figure 3-6 (a) Cross-sectional TEM image of as-grown h-BN/G heterostructure on cobalt foil (Sample D). Evolution of (b) N1s, B1s and (c) C1s peaks as a function of sputtering depth in the depth-profile XPS characterization. (d) Relative atomic concentration of B, C and N versus sputtering depth. (Page 48)

Figure 3-7 Current density versus electric field of 20 Co(foil)/G/h-BN/Co(contact) capacitor devices. All devices have the same size of 250 μm × 250 μm. Inset displays histogram plot of E_{BD}. (Page 50)

Figure 3-8 Specific capacitance as a function of frequency. (Page 51)

Figure 4-1 (a) SEM image of as grown h-BN domains on Co substrate (Sample A), (b) magnified SEM image of one single h-BN domain, (c) schematic illustration of a possible atom arrangement scheme of the three-point star shape domains. (d) Raman spectrum of Sample A. A peak located at 1370cm^{-1} is observed, relating to E_{2g} optical phonon peak of h-BN, (e) B1s XPS, and (f) N1s XPS spectra of Sample A. B1s peak and N1s peak are at 190.6 eV, and 398.0 eV, respectively, indicating the existence of h-BN. (Page 60)

Figure 4-2 (a) Optical microscope image, and (b) SEM image of as grown h-BN/graphene stacked structure (Sample B), (c) AFM image of a transferred h-BN/graphene structure on SiO_2, (d) Raman spectrum of a transferred h-BN/graphene structure on SiO_2. The G/2D peak ratio of graphene indicates the existence of multi-layer graphene. H-BN peak is observed besides G peak. The inset zooms in h-BN peak of 1372 cm^{-1}, relating to E_{2g} optical phonon peak of h-BN, (e), (f), and (g) XPS spectra of C1s, N1s and B1s peaks. (Page 62)

Figure 4-3 Raman mapping of Sample B for a) h-BN E_{2g} peak of h-BN, and b) graphene G peak at one surface area, and c) h-BN E_{2g} peak and d) graphene G peak at another surface area. Insets show Raman spectra accordingly. All scale bars are 1 μm. (Page 64)

Figure 4-4 Schematic of growth mechanism for the MBE growth of h-BN/graphene heterostructure on Co substrate. a) h-BN nucleation on Co substrate, b) initial graphene nucleation on Co substrate and edges of h-BN flakes, c) lateral growth of graphene, d)

layer-by-layer graphene growth on graphene and lateral graphene growth on h-BN flakes.(Page 65)

Figure 5-1 Schematic of the polishing machine. (Page 74)

Figure 5-2 Photographs of (a) unpolished Co foil and (b) polished Co foil. Scratched lines are visible on unpolished Co foil while polished Co foil exhibits a shining surface. (Page 75)

Figure 5-3 (a) SEM image of the polished Co foil and (b) its corresponding EDX spectrum. (Page 75)

Figure 5-4 Optical microscopy images of (a) unpolished Co foil and (b) polished and high-temperature annealed Co foil. AFM images of (c) unpolished and (d) polished and high-temperature annealed Co foils. The RMS roughness is about 231 nm and 11 nm, respectively. The inset in (d) shows an AFM image of a zoomed-in area with a RMS roughness of ~3 nm. (Page 78)

Figure 5-5. SEM images of h-BN films grown on (a) unpolished foil for 900 s (Sample A), and on polished foils for (b) 450 s (Sample B), (c) 900 s (Sample C) and (d) 1800 s (Sample D). The inset in (a) is a magnified image of an h-BN flake on Sample A. (Page 79)

Figure 5-6 Additional SEM images of (a) Sample A, (b) Sample B, (c) Sample C, (d) Sample D. These images were taken with lower magnification compared to those in figure 5-5 in order to show h-BN coverage in larger areas. Insets in (c) and (d) show their corresponding magnified SEM images. (Page 79)

Figure 5-7 SEM (a) and AFM (b) images of an individual h-BN domain from Sample A after transferring on SiO_2/Si substrate. Inset of (b) shows the height profile. (Page 82)

Figure 5-8 SEM (a), AFM (b) and Raman mapping (c) of an individual h-BN domain from Sample C after transferring on SiO_2/Si substrate. Inset of (b) shows the height profile. Inset of (c) is a typical Raman spectrum of transferred h-BN film. (Page 82)

Figure 5-9 SEM images paired with schematic illustrations of h-BN domains with different atomic arrangements: (a, f) triangle shape, (b, g) “kite” shape, (c, h) “hourglass” shape, (d, i) “butterfly” shape and (e, j) multi-apex-star shape. Scale bars in (a)-(e) are 5 µm. (Page 84)

Figure 5-10. (a) Raman spectrum of as-grown h-BN film (Sample D). XPS spectra of (b) N1s and (c) B1s peaks. Current density-electric field characteristics of Co(foil)/h-BN/Co(contact) devices with different contact sizes. Inset shows a schematic of the devices. (Page 85)

Figure 5-11. (a) Optical micrograph and (b) AFM image of the transferred h-BN film (Sample D) on SiO_2. (c) Plan-view TEM image of the transferred h-BN film on a carbon-coated Cu TEM grid. Inset is an electron diffraction pattern, showing six-fold symmetry of the h-BN film. (d) High-resolution TEM image showing multi-layer structure of the h-BN film near its edge. (Page 86)

Figure 5-12. Current density-electric field characteristics of Co(foil)/h-BN/Co(contact) devices with different contact sizes. Inset shows a schematic of the devices. (Page 87)

Figure 5-13 Current-voltage characteristic for a transferred h-BN film on SiO_2/Si substrate. The inset shows a SEM image of the devices for two-point probe measurement. The 100 nm Co layers were deposited as top contacts by a standard photolithography and lift-off process. Both devices (horizontal and vertical) show almost no current flow through the devices in the scanned range of voltage (-5/+5), indicating the insulating nature of h-BN. (Page 88)

List of Tables

Table 2-1 Comparison of sample growth condition. (Page 26)

Table 5-1 Summary of sample growth condition. (Page 77)

Chapter 1: Introduction

1.1 Graphene

Graphene [1-3], known as the world's first discovered and most famous two-dimensional (2D) material has attracted tremendous attention from both academia and industry. In research field, approximately 10,000 journal papers have been published in relative graphene topics every year recently. In addition, the graphene industry is growing up rapidly, including several large and public companies such as Samsung, Intel, Nokia, IBM and Sony. Generally, graphene is composed of a single layer of carbon atoms arranged in a 2D honeycomb lattice, as shown in figure 1-1. The sp2 carbon-carbon covalent bonding length in graphene is about 1.42 Å, which results in a very strong bonding among atoms. For few-layer graphene, the interlayer distance is 3.35 Å, which leads to relatively weak van der Waals (vdW) force. In other word, graphene is a fundamental building block of well-known graphite. Indeed, the discovery of graphene was from the mechanical exfoliation from graphite sheets by "scotch tape" method [1]. Subsequently, it is found that graphene has unique extraordinary properties, such as extremely high carrier mobility [4-5], excellent thermal conductivity [6-7], strong high Young's modulus [8-9], near fully transparent to visible light [10-11] and extreme thinness [12]. Based on these remarkable features, graphene has been predicted as a promising material in a wide range of applications. In fact, a variety of proof-of-concept devices have been studied and demonstrated including high-speed electronic [4, 13] and

optical devices [14], energy generation and storage [15], hybrid materials [16] and chemical sensors [17]. However, due to the zero band gap, graphene itself is not suitable to be used for the fabrication of logical circuits since the current on/off ratio in graphene based field-effect transistors (FETs) is very small to be identified [18]. On the other hand, the synthesis of high-quality and wafer-scale graphene in a controlled manner is still challenging. So far, much effort has been paid to produce graphene such as mechanical exfoliation [1], liquid-phase exfoliation [19], reduction of graphene oxide [20], chemical vapor deposition (CVD) [21-23], surface segregation [24-25], and molecular beam epitaxy (MBE) [26-27]. Despite these efforts, the fine control of the number of graphene layers and structure of graphene sheets over an entire substrate remains a major difficulty. Therefore the optimization of the synthesizing process of graphene with distinct properties is still highly desirable.

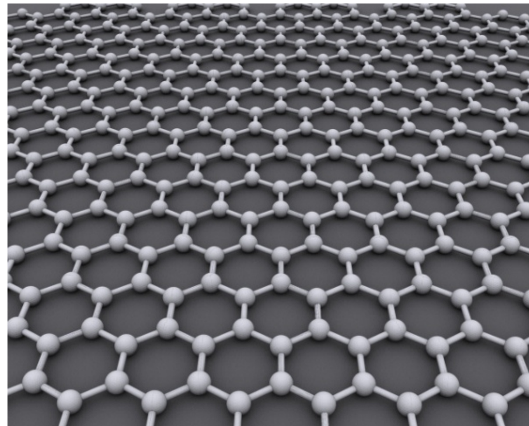

Figure 1-1 Schematic of monolayer graphene. (Source: Wikipedia.org)

1.2 Hexagonal Boron Nitride

Hexagonal boron nitride (h-BN), as called “white graphite”, has a graphene-like in-plane hexagonal lattice structure with both a similar in-plane lattice constant (2.50 Å for h-BN & 2.49Å for graphene) and a similar interlayer distance(3.33 Å for h-BN & 3.35 Å for graphene) [28], which is comprised of alternating boron and nitrogen atoms. Analogous to graphite, boron and nitrogen atoms are bound together by strong covalent sp2 bonds within each 2D h-BN layer, whereas the weak vdW forces occur between different layers. Figure 1-2 shows the schematic of hexagonal structures of h-BN.

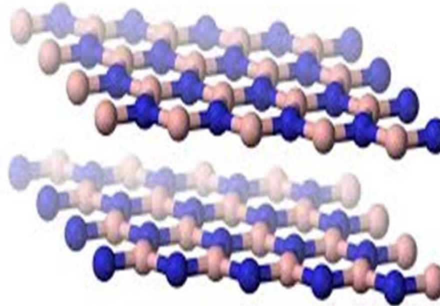

Figure 1-2 Schematic of hexagonal boron nitride layers. (Source: Wikipedia.org)

H-BN films have plenty of attractive properties, such as large band gap (~5.9 eV), high thermal conductivity, excellent thermal and chemical stability, low dielectric constant, high mechanical strength and high hardness, which can be utilized for a great deal of potential applications as both a structural and electronic material [29-32]. For example, h-BN powder is traditionally used as a lubricant [33] and passivation layers [34]. Moreover, due to the wide direct band gap, h-BN provides an alternative way for deep-ultraviolet (DUV) light-emitting devices [35-36]. Besides the optoelectronic applications, h-BN also shows great potential in high-performance electronic devices [5]. In particular,

it was suggested that 2D h-BN is an ideal substrate for graphene and other 2D materials, and can be also served as a good gate dielectric for graphene transistor devices due to a small lattice mismatch (1.7%) with graphene, and an atomically smooth surface that is relatively free of dangling bonds and trapped charges [37-42]. Additionally, graphene on h-BN would give rise to a band gap opening of graphene, and even enhance the carrier mobility by one order of magnitude when compared to graphene on SiO_2 substrate [43-44]. Therefore, it is essential to synthesize wafer-scale and high-quality h-BN films to realize all the potential applications. So far, three major categories have been reported in literature, which are exfoliation [45-47], chemical vapor deposition (CVD) [48-60] and physical vapor deposition (PVD).

1.2.1 Exfoliation

Exfoliation method mainly includes mechanical cleavage and liquid exfoliation which can provide micrometer-sized monolayer or few-layer h-BN flakes.

Since K. S. Novoselov et al developed the famous "scotch tape" method to obtain monolayer graphene, they also reported the synthesis of other 2D materials including h-BN, transition metal dichalcogenides (TMDs) and complex oxides by similar way named as mechanical cleavage [45]. In detail, to extract such 2D flakes, a high-quality bulk crystal material is needed, which can be purchased from commercial companies. Then a fresh surface of a layered crystal would be rubbed against another surface, which can be any solid surface. After this, a variety of flakes would be attached onto the surface, and single layers and few layers flakes can be always found among the resulting flakes. Their

preliminary identification for thicker flakes and other residue was done in an optical microscope. In particular, 2D films become visible on top of a SiO_2 substrate, which shows different contrast for different number of 2D layers.

Coleman et al. [47] firstly reported liquid exfoliation method to produce 2 dmensional nanosheets, such as h-BN and other TMDs. Taking h-BN as an example, firstly, BN powders should be prepared, which are commercially available (e. g. Aldrich). Then the next task is to select the suitable solvents (different material needs different solvent according to relative surface tension). For h-BN, iso-Propyl alcohol (IPA) can be a good candidate. A low power sonic bath and a horn probe sonic tip are needed to carry out the initial sonication. Afterwards, centrifugation process should be done to disperse the flakes in the solvent. It is worth to mention that the quality of nano-material dispersions depends heavily on processing parameters such as sonication time and centrifugation rate. Then the supernatant is decanted to other container and is ready for identifications. In general, TEM is suggested to carefully analyze the flakes, from which, it is possible to estimate the number of layers from the flake edges. Although liquid exfoliation method can bring opportunities of the formation of novel hybrid and composite materials, this method is time-consuming, extremely sensitive to the environment, and incompatible with most solvents.

From the above, mechanical or liquid-phase exfoliation method is a common method used to separate individual sheets from stacked 2D layered crystals by breaking the weak vdW bonds between the layers, which can result in sheets with perfectly crystalline structures. Therefore the sheets produced by this method are used to explore

the intrinsic properties of the materials and basic performance of the related devices. However, exfoliation method can only offer micrometer-sized and atomic-layer-thick h-BN flakes, which are not suitable for large-area production due to the difficulty of controlling the thickness and size of the materials.

1.2.2 CVD

CVD is a process widely used to grow thin films, crystalline or amorphous, from solid, liquid or gaseous precursors of many materials. CVD method has also been extensively explored, in particular, to synthesize 2D layered materials on a large scale with the promise of fine control over the number of layers and the crystalline structures. In fact, CVD has achieved a lot of success on the synthesis of 2D materials, including graphene, h-BN and TMDs. Prior to the present intense interest in h-BN sheets, there have been already many reports of the synthesis of h-BN thin films by CVD methods using various precursors, including independent boron and nitrogen precursors such as BF_3/NH_3 [48], BCl_3/NH_3 [49] B_2H_6/NH_3 [50-51] and triethylboron (TEB)/NH_3 [52]. Recently, a single precursor such as ammonia borane (BH_3NH_3) [32, 34, 39] and borazine $(HBNH)_3$ [37, 53] are most used to synthesize h-BN layers due to their natural advantage of having a 1:1 B/N stoichiometry. In addition, the main difference for the various precursor types is the gas delivery system. For example, other than directly introducing the gas source into the chamber, for solid (e. g. BH_3NH_3) or liquid precursors (e. g. $(HBNH)_3$), the solid or liquid can be vaporized (heat treatment) and then transported to the deposition chamber. The transport of the precursor can also be assisted by a carrier

gas, such hydrogen (H_2) or NH_3. In the case of independent gas source, control of the ratio between the boron source and nitrogen source become critical. In addition, there are many different types of CVD processes, such as plasma enhanced (PECVD), atmospheric pressure (APCVD), low pressure (LPCVD), ultra-high vacuum (UHVCVD) and many more. As for h-BN growth, APCVD and LPCVD are most used. Furthermore, a wide range of transition catalyst metals, including Cu [32, 39, 54] Pt [55-57], Ni [34, 58] and Co [59] polycrystalline films and foils, as well as on Fe [37, 53], Pd [60] and Pt [61] single crystals, have been reported to be used as substrates. Since each of individual CVD growth is different in aspect of growth temperature, flow rate, growth time and many other parameters, the details of the growth process are not summarized here. In summary, CVD growth has made significant progress in h-BN synthesis, and the optimization of CVD growth for wafer-scale crystalline 2D h-BN films toward a controllable and scalable way is still undergoing.

1.2.3 PVD

Besides the popular CVD method, PVD method, such as pulsed laser deposition (PLD) [62], reactive magnetron sputtering [63] and ion beam sputtering deposition (IBSD) [64-65], were also attempted to synthesize h-BN layers. PLD is an alternative PVD technique, where a high energy, focused laser beam pulse causes rapid heating on the face of the target, causing both ionized and neutral components to accelerate from the target in the form of a plasma plume normal to the target surface. Depending on the pressure and target-to-surface distance, it may happen that the plasma can be thermalized

by collisions with the background gas. For h-BN growth, amorphous boron nitride and nitrogen background gas are usually used. In contrast to CVD processes, PLD technique has achieved h-BN growth on non-metal substrate such as highly ordered pyrolytic graphite (HOPG) and sapphire, which opens up the possibility of preparing high-quality BN films on a wide range of substrates.

Reactive magnetron sputtering has been used to grow epitaxial metals, compounds, and semiconductor heterostructures for a long period. Recently, this method has also been utilized to develop the growth of atomic h-BN films using reactive magnetron sputtering of boron in N_2/Ar atmosphere. In contrast to PLD process, the boron atoms are evaporated by collision cascades due to the impact of energetic Ar+ ions on a solid boron target, and nitrogen plasma is generated by reactive radio frequency (RF). B and N species tend to assemble into a well-ordered film consisting of layered atomic h-BN sheets. IBSD can be defined as a facile and innovative sputtering method. A high energy Ar ion beam to sputter h-BN target was used to grow few-layer h-BN films.

Compared to CVD, PVD growth avoids the use of unconventional precursors and it is also much easier to control, which should be very useful for the large-scale production of h-BN.

1.3 Heterostructures based on graphene and h-BN

Van der Waals materials have received high interest recently for their novel properties and high potential in various device applications, such as graphene [37], h-BN [43-44] and MoS_2 [37]. For exploring new paradigm in the 2D devices, heterostructures

which are made from a combination of alternating layers of graphene, h-BN, MoS_2 and other 2D materials, provide a platform to investigate novel phenomenon in fundamental physics. Among those heterostructures, research on in-plane and vertically-stacked heterostructures of graphene and h-BN has attracted intense attentions for energy band engineering and device performance optimization of graphene because of the small lattice mismatch (~1.7%) between graphene and h-BN, the conducting nature of graphene and the insulating nature of h-BN [66-67]. For example, graphene-based transistors using h-BN as a gate insulator and supporting substrate have shown significantly enhanced field-effect carrier mobility [5]. In addition, theoretical calculations predicted that an obvious band gap opening could be realized in the in-plane h-BN and graphene hybrids/heterostructures as well as with relatively higher carrier mobility [68]. This makes h-BN-G as a promising 2D material for graphene-based nanoelectronics. Furthermore, some unique physical phenomena were detected on the vertically stacked graphene/h-BN systems such as the Hofstadter butterfly effect and quantum Hall effect [69-70]. Briefly, both in-plane and vertically stacked heterostructures of h-BN and graphene have shown a lot of intriguing properties and opened up a wide range of new scientific interests.

Traditionally, both graphene and h-BN films can be obtained by mechanical exfoliation method and assembled into vertical heterostructures by dry-transfer method [69]. However, the thickness and size of such samples are difficult to control and the effect of surface contamination on the material/device properties is still unclear. On the other hand, CVD has been used to provide an alternative approach for the preparation of

h-BN/Graphene heterostructures. For example, CVD growth of h-BN (or Graphene) on mechanically exfoliated Graphene (or h-BN) as well as two-step CVD growth for both G and h-BN have been reported to obtain h-BN and graphene-based heterostructures [66-67, 71-73]. The lateral hybrid heterostructures can also be formed by step-by-step patterned re-growth method [66]. Although significant progress has been made for these heterostructures, it is still challenging to controllably and scalably synthesize large-area, high-quality graphene/h-BN based heterostructures.

1.4 Motivation of 2D materials growth by molecular beam epitaxy

From the discussion above, it is evident that 2D materials are very promising for the next generation nanoelectronics and nanophotonics. Meanwhile, it is crucial to develop a controllable and scalable process to synthesize those 2D films. Among the various approaches to synthesizing 2D films, molecular beam epitaxy (MBE) can offers precise control over growth conditions thanks to its ultra-high vacuum (UHV) environment, atomic layer epitaxy accuracy and controllability, instant introduction and control of multiple sources, ease of doping of materials and in-situ layer-by-layer characterization. For CVD process, the growth rate may change dramatically with the exposed surface area of the catalytic substrate, while MBE does not have such constraints. As known, catalyst-free growth is crucial for vertically stacked heterostructures since the existing as-grown layers will serve as substrate for sequential growth [74-75]. Therefore, MBE is promising for the in-situ growth of vertically stacked heterostructures with defect-free interfaces due to the absence of catalytic processes. In addition, instant introduction and

control of multiple sources using automated shutter control can allow the growth of alloys with multiple elements for band gap engineering and short-period superlattices. On the other hand, in contrast to using very high temperature to break the gas molecules for growth in CVD, MBE can take advantage of plasma or electron cyclotron resonant processes, which can enable film synthesis at a relatively lower substrate temperature. This relatively lower temperature process can avoid the happening of ripples or wrinkles in the thin film growth due to thermal strain effect, which can minimize material inter-diffusion and form a very sharp interface in the heterostructures. Finally, direct doping of these growing layers in MBE system would be possible from molecular beams using appropriate effusion cells or other atomic sources, which may result in some new materials with promising properties, such as boron carbon nitride (BCN). Therefore, it is believed that MBE growth is very promising to bring new opportunities to develop integrated 2D materials system.

1.5 Chapter arrangement

In this dissertation, the growth of graphene, h-BN and their vertical and lateral heterostructures by molecular beam epitaxy (MBE) is mainly studied. In addition, the growth mechanism, fundamental physics and possible applications are also discussed.

In chapter 2, in-situ epitaxial growth of graphene/h-BN heterostructures on Co film substrate was achieved by using plasma-assisted MBE. The direct graphene/h-BN vertical stacking structures were demonstrated and further confirmed by various characterizations, such as Raman spectroscopy, SEM, XPS and TEM. Large area

heterostructures consisting of single-layer/bilayer graphene and multilayer h-BN were achieved. The mismatch angle between graphene and h-BN is below 1°.

In chapter 3, the growth of graphene/h-BN heterostructures on Co foil substrate by plasma-assisted MBE is discussed. It is found that the coverage of h-BN layers on the epitaxial graphene is growth-time dependent. Large-area, uniform-quality graphene/h-BN heterostructures were achieved. Capacitor devices with Co(foil)/G/h-BN/Co(contact) configuration were fabricated to evaluate the dielectric properties of h-BN. The measured breakdown electric field showed a high value of 2.5-3.2 MV/cm. Both I-V and C-V characteristics indicated that the epitaxial h-BN film is of good insulating characteristics.

In chapter 4, the lateral growth of graphene on in situ epitaxial h-BN flakes by plasma-assisted MBE was studied. Single-crystal h-BN domains were grown on Co film substrates at a substrate temperature of 850~900 ^{o}C. Three-point star shape h-BN domains were observed by SEM, and the B-N bonds were confirmed by Raman and XPS. In addition, the lateral growth mechanism is discussed. The h-BN flakes on Co surface can be a template used for sequential growth of multilayer graphene, leading to an h-BN/graphene heterostructure.

In chapter 5, it mainly studied the growth of large-area and multi-layer h-BN layers on polished Co foils by plasma-assisted MBE. The coverage of h-BN layers can be readily controlled by growth time under appropriate growth conditions. The multi-layer h-BN film is confirmed by various characterizations. Dielectric property of as-grown h-BN film is evaluated by characterization of Co(foil)/h-BN/Co(contact) capacitor devices. Breakdown electric field is in the range of 3.0-3.3 MV/cm, which indicates that the

epitaxial h-BN film has good insulating characteristics. In addition, the effect of substrate morphology on h-BN growth is discussed regarding different domain density, lateral size, and thickness of the h-BN films grown on unpolished and polished Co foils.

In the end, a conclusion of this dissertation is summarized in chapter 6.

Reference

[1] K. S. Novoselov, A. K. Geim, S. V. Morozov, D. Jiang, Y. Zhang, S. V. Dubonos, I. V. Grigorieva and A. A. Firsov, Science 306, 666-669(2004).

[2] K. S. Novoselov, A. K. G., S. V. Morozov, D. Jiang, M. I. Katsnelson, I. V. Grigorieva, S. V. Dubonos and A. A. Firsov. Nature 438, 197-200(2005).

[3] Y. Zhang, Y.-W. T., H. L. Stormer and P. Kim. Nature 438, 201-204(2005).

[4] X. Du, I. Skachko, A. Barker and E.Y. Andrei, Nat. Nanotechnol. 3, 491-495(2008).

[5] C. Dean, A. Young, I. Meric, C. Lee, L. Wang, S. Sorgenfrei, K. Watanabe, T. Taniguchi, P. Kim, K. L. Shepard and J. Hone, Nat. Nanotechnol. 5, 722-726(2010).

[6] A. A. Balandin , S. Ghosh , W. Z. Bao , I. Calizo , D. Teweldebrhan , F. Miao and C. N. Lau , Nano Lett. 8, 902-907(2008).

[7] A. A. Balandin, Nat mater. 10, 569–581(2011).

[8] C. Lee, X. Wei, J .W. Kysar and J. Hone, Science 321, 385-388(2008).

[9] S. P. Koenig, N. G. Boddeti, M. L. Dunn and J. Scott Bunch. Nat. nanotechnol. 6, 543-546(2011).

[10] P. Blake, E. W. Hill, A. H. Castro Neto, K. S. Novoselov, D. Jiang, R. Yang, T. J. Booth and A. K. Geim, Appl. Phys. Lett. 91, 063124(2007).

[11] R. R. Nair, P. Blake, A. N. Grigorenko, K. S. Novoselov, T. J. Booth, T. Stauber, N. M. R. Peres and A. K. Geim, Science 320, 1308(2008).

[12] Z. H. Ni, H. M. Wang, J. Kasim, H. M. Fan, T. Yu, Y. H. Wu, Y. P. Feng and Z. X. Shen, Nano Lett. 7, 758-2763(2007).

[13] Y. M. Lin, C. Dimitrakopoulos, K. A. Jenkins, D. B. Farmer, H. Y. Chiu, A. Grill and P. Avouris, Science 327, 662(2010).

[14] M. Liu, X. B. Yin, E. Ulin-Avila, B. S. Geng, T. Zentgraf, L. Lu, F. Wang and X. Zhang, Nature 474, 64-67(2011).

[15] K. S. Kim, Y. Zhao, H. Jang, S. Lee, J. Kim, K. Kim, J. Y. Ahn, P. Kim, J. Y. Choi and B. H. Hong, Nature 457, 706-710(2009).

[16] X. Yang, M. S. Xu, W. M. Qiu, X. Q. Chen, M. Deng, J. L. Zhang, H. Iwai, E. Watanabe, and H. Chen, Mater. Chem. 21, 8096-8103(2011).

[17] A. Geim, Nat. Mater. 6, 183-191(2007).

[18] Kim, K.; Choi, J. Y.; Kim, T.; Cho, S. H. and Chung, H. J. Nature 479, 338(2011).

[19] Y. Hernandez, V. Nicolosi, M. Lotya, F. M. Blighe, Z. Sun, S. De, I. T. McGovern, B. Holland, M. Byrne, J. J. Boland, et al., Nat. Nanotechnol. 3, 563-568(2008).

[20] S. Pei, S. and H. M. Cheng, Carbon, 50, 3210-3228(2012).

[21] Q. Yu, J. Lian, S. Siriponglert, H. Li, Y. P. Chen and S. –S. Pei, Appl. Phys. Lett. 93, 113103(2008).

[22] A. Reina, X. Jia, J. Ho, D. Nezich, H. Son, V. Bulovic, M. S. Dresselhaus and J. Kong, Nano Lett. 9, 30(2009).

[23] X. Li, W. Cai, J. An, S. Kim, J. Nah, D. Yang, R. Piner, A. Velamakanni, I. Jung, E. Tutuc, et al., Science 324, 1312(2009).

[24] M. Rubio-Roy, F. Zaman, Y. Hu, C. Berger, M. W. Moseley, J. D. Meindl, and W. A. de Heer, Appl. Phys. Lett. 96, 082112(2010).

[25] C. Berger, Z. Song, T. Li, X. Li, A. Y. Ogbazghi, R. Feng, Z. Dai, A. N. Marchenkov, E. H. Conrad, P. N. First, and W. A. de Heer, J. Phys. Chem. B, 108 (52), 19912(2004).

[26] N. Zhan, G. Wang and J. Liu, Appl. Phys. A 105, 341-345(2011).

[27] N. Zhan, M. Olmedo, G. Wang and J. Liu,Carbon 49, 2046-2052(2011)

[28] R. T. Paine and C. K. Narula, Chem. Rev. 90, 73-91 (1990).

[29] A. Nag, K. Raidongia, R. Datta, K. P. S. S. Hembaram, U. V. Waghmare and C. N. Rao, ACS Nano. 4, 1539-1544(2010).

[30] L. Liu, Y. P. Feng, Z. X. Shen, Phys. Rev. B 68, 104102 (2003).

[31] K. Watanabe, T. Taniguchi and Kanda H., Nat. Mater. 3, 404-409 (2004).

[32] L. Song, L. Ci, H. Lu, P. Sorokin, C. Jin, J. Ni, A. Kvashnin, D. Kvashnin, J. Lou, B. Yakobson and P. Ajayan, Nano Lett. 8, 3209-3215 (2010).

[33] Y. Kimura, T. Wakabayashi, K. Okada, T. Wada and H. Nishikawa, Wear 232, 199-206 (1999).

[34] Z. Liu, Y. Gong, W. Zhou, L. Ma, J. Yu, J. C. Idrobo, J. Jung, A. H. MacDonald, R. Vajtai, J. Lou and P. M. Ajayan, Nat. Commun. 4, 2541(2013).

[35] K. Watanabe, T. Taniguchi and H. Kanda, Nat. Mater. 3, 404-409 (2004).

[36] K. K. Kim, S. M. Kim and Y. H. Lee, J. Kor. Phys. Soc. 64, 1605-1616 (2014).

[37] S. M. Kim, A. Hsu, M. Park, S. Chae, S. Yun, J. Lee, D. Cho, W. Fang, C. Lee, T. Palacios, M. Dresselhaus, K. K. Kim, Y. H. Lee, and J. Kong, Nat. Commun. 6, 8662(2015).

[38] A. Yan, J. Velasco Jr, S. Kahn, K. Watanabe, T. Taniguchi, F. Wang, M. F. Crommie and A. Zettl, Nano Lett. 15, 6324-6331(2015).

[39] S. Wang, X. Wang and J. H. Warner, ACS Nano 9, 5246-5254(2015).

[40] M. Okada, T. Sawazaki, K. Watanabe, T. Taniguch, H. Hibino, H. Shinohara and R. Kitaura, ACS Nano 8, 8273-8277(2014).

[41] L. Britnell, R. V. Gorbachev, R. Jalil, B. D. Belle, F. Schedin, A. Mishchenko, T. Georgiou, M. I. Katsnelson, L. Eaves and S. V. Morozov, Science 335, 947-950(2012).

[42] L. Wang, B. Wu, J. Chen, H. Liu, P. Hu and Y. Liu, Adv. Mater. 26, 1559-1564(2014).

[43] W. Gannett, W. Regan, K. Watanabe, T. Taniguchi, M. F. Crommie and A. Zettl, Appl. Phys. Lett. 98, 242105 (2011).

[44] E. Kim, T. Yu, E. Sang Song and B. Yu, Appl. Phys. Lett. 98, 262103(2011).

[45] K. S. Novoselov, D. Jiang, F. Schedin, T. J. Booth, V. V. Khotkevich, S. V. Morozov and A. K. Geim, Proc. Natl Acad. Sci. 102, 10451(2005).

[46] D. Pacilé, J. C. Meyer, Ç. Ö. Girit and A. Zettl. Appl. Phys. Lett. 92, 133107(2008).

[47] J. N. Coleman, M. Lotya, A. O'Neill, S. D. Bergin, P. J. King, U. Khan, K.Young, A. Gaucher, S. De, R. J. Smith et al., Science 331, 568-571 (2011).

[48] H. O. J. Pierson, Compos. Mater. 9, 228-240(1975).

[49] A. S. Rozenberg, Y. Sinenko and N. Chukanov, J. Mater. Sci. 28, 5528-5533(1993).

[50] S. Middleman, Mater. Sci. Eng., A 163, 135-140(1993).

[51] A. Ismach, H. Chou, D. A. Ferrer, Y. Wu, S. McDonnell, H. C. Floresca, A. Covacevich, C. Pope, R. Piner, M. J. Kim, R. M. Wallace, L. Colombo and R. S. Ruoff, ACS Nano 6, 6378-6385(2012)

[52] Q. S. Paduano, M. Snure, J. Bondy and T. W. C.Zens, Appl. Phys. Express, 7, 071004(2014).

[53] S. Caneva, R. S. Weatherup, B. C. Bayer, B. Brennan, S. J. Spencer, K. Mingard, A. Cabrero-Vilatela, C. Baehtz, A. J. Pollard and S. Hofmann, Nano Lett. 15, 1867-1875(2015).

[54] K. Lee, H.-J. Shin, J. Lee, I. Lee, G.-H. Kim, J.-Y. Choi and S.-W Kim, Nano Lett. 12, 714−718(2012).

[55] G. Kim, A. Jang, H. Y. Jeong, Z. Lee, D. J. Kang and H. S. Shin, Nano Lett. 13, 1834-1839(2013).

[56] Y. Gao, W. Ren, T. Ma, Z. Liu, Y. Zhang, W. Liu, L.-P. Ma, X. Ma and H.-M. Cheng, ACS Nano 7, 5199-5206(2013).

[57] J.-H. Park, J. C. Park, S. J. Yun, H. Kim, D. H. Luong, S. Kim, S. Choi, W. Yang, J. Kong, K. K. Kim and Y. H. Lee, ACS Nano 2014, 8, 8520-8528(2014).

[58] Kong, J. Y. Shi, C. Hamsen, X. Jia, K. K. Kim, A. Reina, M. Hofmann, A. L. Hsu, K. Zhang, H. Li, Z.-Y. Juang, M. S. Dresselhaus, L.-J. Li and J. Kong, Nano Lett. 10(10), 4134-4139(2010).

[59] C. M. Orofeo, S. Suzuki, H. Kageshima and H. Hibino, Nano Research 5, 335-347(2013).

[60] M. Morscher, M. Corso, T. Greber and J. Osterwalder, Surf. Sci. 600, 3280-3284(2006).

[61] E. Ćavar, R. Westerström, A. Mikkelsen, E. Lundgren, A. Vinogradov, M. L. Ng, A. B. Preobrajenski, A. A. Zakharov and N. Mårtensson, Surf. Sci. 2008, 602, 1722-1726(2008).

[62] N. R. Glavin, M. L. Jespersen, M. H. Check, J. Hu, A. M. Hilton, T. S. Fisher and A. A. Voevodin, 572, 6-11(2014).

[63] J. Meng, X. Zhang, H. Wang, X. Ren, C. Jin, Z. Yin, X. Liu and H. Liu, Nanoscale 7, 16046-16053(2015).

[64] P. Sutter, J. Lahiri, P. Zahl, B. Wan and E. Sutter, Nano Lett. 13, 276-281(2012).

[65] H. Wang, X. Zhang, J. Meng, Z. Yin, X. Liu, Y. Zhao and L. Zhang, Small 11, 1542-1547(2015).

[66] Z. Liu, L. Ma, G. Shi, W. Zhou, Y. Gong, S. Lei, X. Yang, J. Zhang, J. Yu, K. P. Hackenberg, A. Babakhani, J-C. Idrobo, R. Vajtai, J. Lou and P. M. Ajayan, Nat. Nanotechnol. 8, 119-124(2013).

[67] W. Yang, G. Chen, Z. Shi, C. Liu, L. Zhang, G. Xie, M. Cheng, D. Wang, R. Yang, D. Shi, K. Watanabe, T. Taniguchi, Y. Yao, Y. Zhang and G. Zhang, Nature mater. 12, 792-797(2013).

[68] J. Y. Wang , R. Q. Zhao , Z. F. Liu and Z. R. Liu , Small 9 , 1373-1378(2013).

[69] W. Yang, G. Chen, Z. Shi, C. C. Liu, L. Zhang, G. Xie, M. Cheng, D. Wang, R. Yang, D. Shi, K. Watanabe, T. Taniguchi, Y. Yao, Y. Zhang and G. Zhang, Nat. Mater. 12, 792-797(2013).

[70] C. R. Dean, L. Wang, P. Maher, C. Forsythe, F. Ghahari, Y. Gao, J. Katoch, M. Ishigami, P. Moon, M. Koshino, T. Taniguchi, K. Watanabe, K. L. Shepard, J. Hone and P. Kim, Nature, 497, 598-602(2013).

[71] Z. Liu, L. Song, S. Zhao, J. Huang, L. Ma, J. Zhang, J. Lou and P. M. Ajayan, Nano Lett. 11, 2032-2037(2011).

[72] T. Gao, X. Song, H. Du, Y. Nie, Y. Chen, Q. Ji, J. Sun, Y. Yang, Y. Zhang and Z. Liu, Nat. Commun. 6. 6835(2015).

[73] Q. Wu, S. K. Jang, S. Park, S. J. Jung, H. Suh, Y. H. Lee, S. Lee and Y. J. Song, Nanoscale 7, 7574-7579(2015).

[74] S.Nakhaie, J. M. Wofford, T. Schumann, U. Jahn, M. Ramsteiner, M. Hanke, J. Lopes and H. Riechert, Appl. Phys. Lett. 106, 213108(2015).

[75] Z. Zuo, Z. Xu, R. Zheng, A. Khanaki, J. Zheng and J. Liu, Sci. Rep., 5, 14760 (2015).

Chapter 2: In-situ epitaxial growth of graphene/h-BN heterostructures on Co film substrate using plasma-assisted MBE

2.1 Introduction

As introduced in chapter 1, vdW materials have received high interest recently for their novel properties and high potential in various device applications [1-3]. While graphene is one of the most prominent vdW members, beyond graphene materials such as MoS_2, ZnSe, and hexagonal boron nitride (h-BN) are also being eagerly investigated [4-11]. For exploring new paradigm in the 2D devices, atomic-scale heterostructures, which are made from a combination of alternating layers of graphene, h-BN, MoS_2 and so on, have been paid a great deal of attention. Such heterostructures provide a platform to investigate novel phenomenon in fundamental physics, and there are reports indicating superior properties for device applications [12-15]. Among these vdW heterostructures, the stacking of h-BN with another vdW layer, in particular, graphene [16, 17], is of imminent interest. H-BN has a hexagonal crystal structure similar to graphene's with less than 2% lattice mismatch [18]. H-BN is a dielectric with a dielectric constant of about 4 [19] and a wide band gap of ~5.9 eV [7]. H-BN also has exceptional thermal and chemical stabilities [10]. These properties enable h-BN as an excellent chemical and electrical barrier material for graphene and other vdW materials.

To obtain such heterostructures, mechanical exfoliation and chemical vapor deposition (CVD) growth were widely used [20-22]. Much success has been achieved. Nevertheless, direct deposition of high-quality, wafer-scale vdW heterostructures remains challenging. Therefore, non-CVD approaches have been proposed recently, for example, a plasma-assisted deposition method has been used to achieve epitaxial growth of single-domain graphene on h-BN [23]. As a versatile tool, MBE has natural advantages in high-quality heterostructure growth thanks to its UHV environment, atomic layer epitaxy accuracy and controllability, instant introduction and control of multiple sources, easy of doping of materials and in situ layer-by-layer characterization. As a matter of fact, vdW epitaxy was first demonstrated using MBE process [24-25]. Most recently, MBE has also been used to successfully synthesize single-layer and bilayer graphene [26-29]. In this paper, we demonstrate a solution for fabricating vdW heterostructures. Graphene/h-BN heterostructures were synthesized on cobalt substrates by using MBE. Various characterizations were carried out to evaluate the heterostructures. Wafer-scale heterostructures consisting of single-layer/bilayer graphene and multilayer h-BN were achieved. The mismatch angle between graphene and h-BN is below 1°.

2.2 Material growth, device fabrication and characterization method

Thermally oxidized Si wafers with a SiO_2 layer of 300 nm were used as substrates. They were transferred to an E-beam evaporator system for the deposition of a Co film of 400 nm. The wafers were subsequently loaded on to standard 3” wafer MBE holders and transferred to the growth chamber for growth. A Knudsen effusion cell filled with B_2O_3

powder (Alfa Aesar, 99.999%) was used as B source. A thermocracker was used to crack acetylene gas (Airgas, 99.999%) as C source. The C source was tuned by either acetylene gas flow or cracker temperature. An electron cyclotron resonance (ECR) system was used to form nitrogen gas plasma (Airgas, 99.9999%) as N atomic source. The N source was tuned by either nitrogen gas flow or ECR magnetron current.

For a typical growth, the substrate is firstly annealed at 800~850 ºC under a hydrogen flow of 10 sccm for a duration of 30 minutes. At the end of substrate surface treatment, the hydrogen gas flow is stopped and substrate temperature is further ramped up to 870~900 ºC for graphene/h-BN heterostructure growth. The thermal cracker temperature is ramped to 1200 ºC and 3 sccm acetylene is introduced into the chamber for graphene growth. The growth lasts from 10 s to 1 minute. Subsequently, h-BN growth follows with minimal time gap. B cell temperature is precisely ramped to 900~1100 ºC right before h-BN layer growth. Nitrogen flow rate is 10 sccm and the growth lasts 10~15 minutes. At the end of h-BN growth, the substrate temperature is slowly cooled down towards room temperature at a rate of 10 ºC/min. The slow substrate cooling process suggests that the epitaxy undergoes layer-by-layer growth mode, which is in contrast to fast cooling procedure with much higher cooling rates in the growth of graphene by precipitation of carbon atoms from the metal substrate in some CVD process [30-31].

Raman characterizations were performed using a HORIBA LabRam system equipped with a 50-mW 514-nm green laser. Scanning electron microscopy (SEM) images were acquired using a Philips XL30-FEG system. X-ray photoelectron spectroscopy (XPS) was carried out using a Kratos AXIS ULTRA XPS system equipped

with an Al Kα monochromatic X-ray source and a 165 mm mean radius electron energy hemispherical analyzer. Transmission electron microscopy (TEM) images and electron diffraction patterns were acquired using a FEI/Philips CM-30 TEM. Cross sectional TEM sample was prepared using focused ion beam technique. The graphene/h-BN thin film was covered by an Ir layer and further protected by electron-beam and ion-beam deposited Pt layers. Plan-view TEM sample was prepared using direct transfer method. After spin coated with PMMA, the sample was submerged in $FeCl_3$ solution to etch away the Co metal layer. The film was then transferred onto carbon coated Cu TEM grid and treated with acetone and DI water to remove PMMA. For fabricating back-gate MOSFET, the film was transferred onto an oxidized silicon substrate with a 300nm SiO_2 layer by using the same PMMA-assisted method, then photolithography was done to form the pattern. Then, SF_6 gas was used to etch away h-BN to expose graphene. After that, a 10/70nm Ti/Au contact was deposited.

2.3 Results and discussion

As grown vdW thin films are transparent and thus not visible for bare eye or through optical microscope (Figure 2-1 (a)). There are some surface imperfections, possibly a result from the high temperature growth. H-BN domains are of large scale and transparent. As the samples are imaged by SEM, a surface contrast is observed in secondary electron image because secondary electron signals from h-BN and graphene/Co substrate have different intensity. Figure 2-1 (b) shows an SEM image of a graphene/h-BN sample (Sample A) on which large triangular domains of ~20 μm are

observed. Despite the underlying very rough Co substrate surface, which consists of small grains due to heat treatment, wafer-scale graphene has been grown, followed by the formation of the triangular shaped h-BN domains as inferred by both optical microscope imaging and Raman scattering results (Figure 2-2).

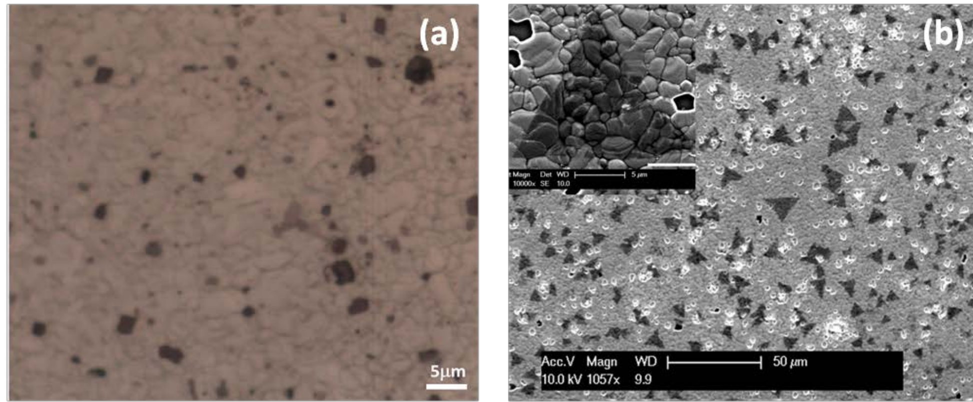

Figure 2-1 (a) Optical microscopy image of graphene/h-BN heterostructure sample (b) SEM image of graphene/h-BN heterostructure on cobalt substrate (Sample A). Inset is taken under the same condition with larger magnification, and it shows a large triangular h-BN flake of about 20 μm. The background is the rough substrate surface with packed Co grains resulted from heat treatment.

In order to achieve continuous wafer-scale h-BN single domain instead of discrete flakes, fine-tuning of the sample growth condition was performed by reducing high-temperature substrate treatment duration, graphene layer thickness, and growth temperature for h-BN layer. Detailed difference in growth condition is listed in Table 1. The resulting sample (Sample B) shows smoother surface morphology under optical microscopy (Figure 2-3 (a)). The shorter growth time and thinner graphene layer clearly improve h-BN layer growth. Sample B exhibits the graphene/h-BN film that covers the entire sample surface, and triangular h-BN domains are no longer visible (Figure 2-3 (b)). Further characterizations were based on this heterostructure sample.

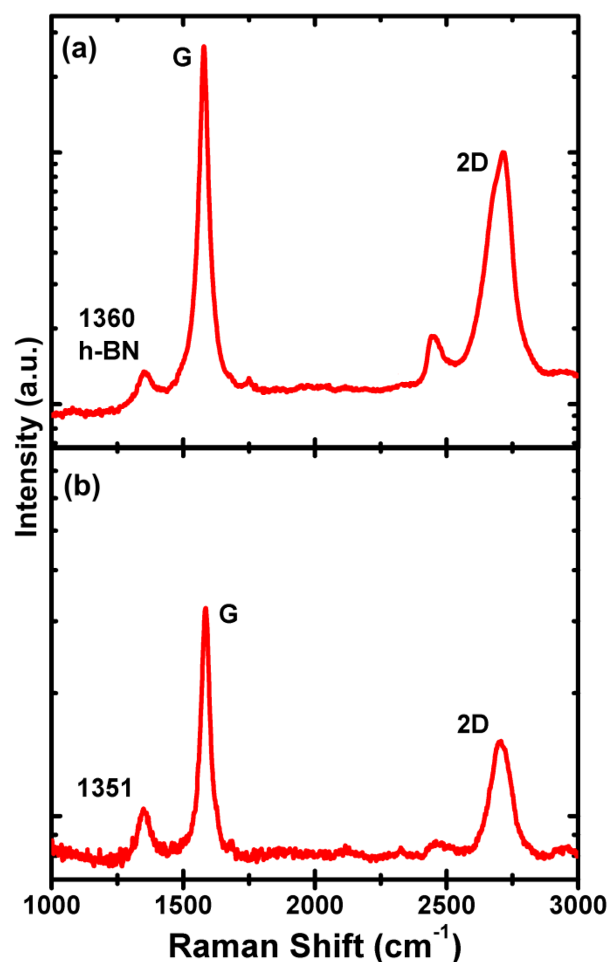

Figure 2-2 (a) and (b) are typical graphs with (a) showing both h-BN E_{2g} optical phonon peak at 1360 cm^{-1} and signature graphene G and 2D peaks at discrete locations, and (b) showing only graphene peaks across the entire surface.

Step	Parameters	Sample A	Sample B
Pre-growth Annealing	**Temperature**	**800 °C**	**850 °C**
	Duration	**40 minutes**	**10 minutes**
Graphene Growth	**Substrate temperature**	**800 °C**	**850 °C**
	Gas flow	**3 sccm**	**3 sccm**
	Cracker temperature	**1200 °C**	**1000 °C**
	Growth duration	**1 minute**	**10 s**
H-BN Growth	**Substrate temperature**	**900 °C**	**850 °C**
	Boron cell temperature	**1000 °C**	**950 °C**
	Nitrogen gas flow	**10 sccm**	**10 sccm**
	Nitrogen ECR current	**50 mA**	**60 mA**
	Growth duration	**15 minutes**	**10 minutes**

Table 2-1 Comparison of sample growth condition

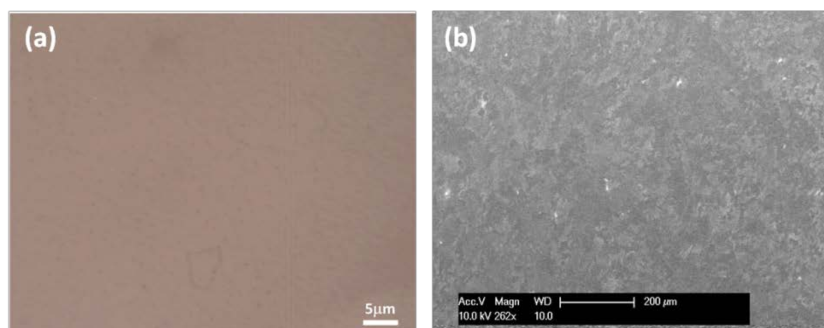

Figure 2-3 (a) Optical microscopy image and SEM image (b) of graphene/h-BN sample with wafer-scale coverage (Sample B).

Figure 2-4 (a) shows an XPS survey scan spectrum, with the peaks of interest circled. Fine scans were performed in these sites and evident energy peaks for B, C, and N were observed. Figure 2-4 (b), (c) and (d) show XPS spectrum of B1s, C1s, and N1s state, respectively. C1s peak is observed at a position of 284.5 eV, which is smaller than environmental C1s peak in XPS, and is closer to the sp^2 C-C bond at 284.0 eV [32]. This is an indication of graphene. B1s and N1s exhibit an energy position at 398.0 eV and 190.6 eV, respectively, which are typical characteristics of h-BN [33]. Based on integrated peak intensity and corrections, B/N ratio was estimated to be 1.1 from the surface of h-BN, indicating that the growth of h-BN is slightly B-rich.

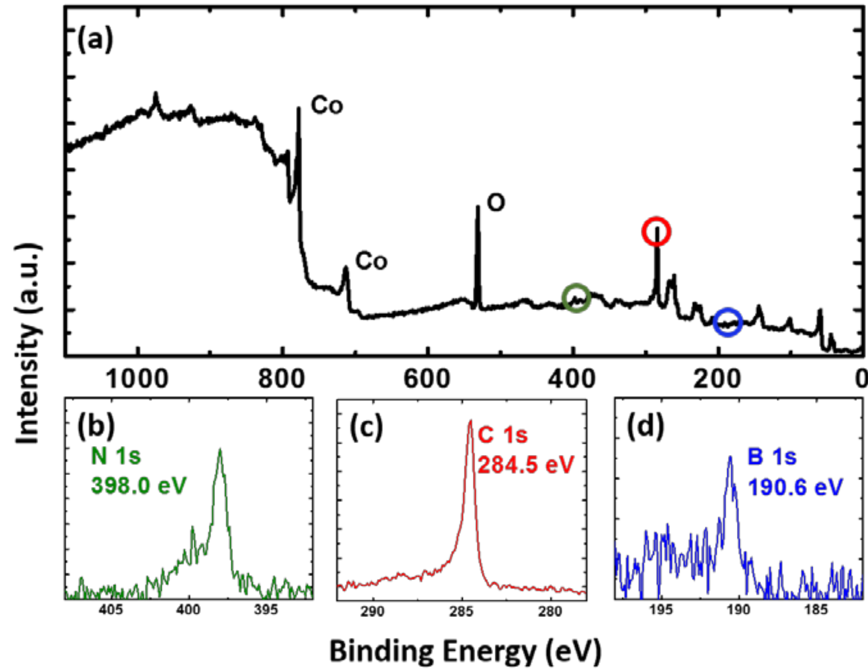

Figure 2-4 XPS spectra of graphene/h-BN heterostructure on Co substrate (Sample B). a) Survey spectrum, b) N1s peak, c) C1s peak, and d) B1s peak. B1s and N1s are at 190.6 eV, and 398.0 eV, respectively, indicating the existence of h-BN. C1s peak is at 284.5 eV, indicating the presence of graphene.

Figure 2-5 shows Raman spectrum of the sample. The G/2D peak ratio of the graphene signals indicates the existence of single-layer/bilayer graphene. The inset is a spectrum near the graphene D peak, which lies at 1356 cm^{-1}. The appearance of D peak has been observed in other reports of graphene/h-BN heterostructure [34]. In addition, an h-BN E_{2g} optical phonon peak is evident at 1364 cm^{-1}. Analyzing the 2D peak of graphene to detect the mismatch angle of graphene and h-BN has been reported recently [35]. In this experiment, the FWHM of the 2D peak of as grown sample is 38 cm^{-1}, which indicates the mismatch angle is below 1°.

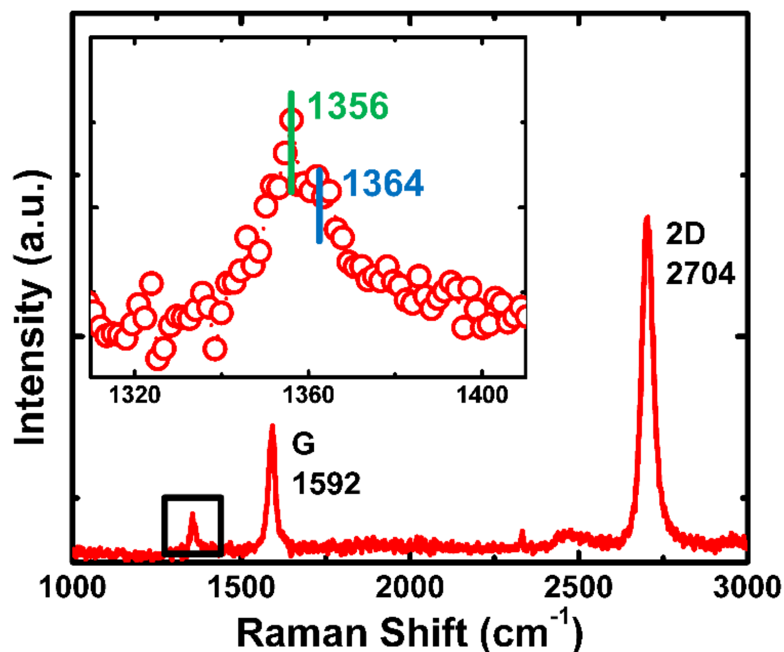

Figure 2-5 Raman spectrum of graphene/h-BN heterostructure (Sample B). Evident graphene G and 2D peaks are observed, with their intensity ratio indicating 1~2 layer graphene. The inset is enlarged spectrum in the 1300~1400 cm^{-1} region. Two peaks are resolved, relating to graphene D mode and E_{2g} optical phonon peak of h-BN, respectively.

Figure 2-6 (a) shows a plan-view TEM image of the transferred graphene/h-BN heterostructure. Continuous thin film is observed with some areas folded. Black spots originate from PMMA residue during film transfer process. Figure 2-6 (b) shows a selected area electron diffraction (SAED) pattern of the plan-view graphene/h-BN heterostructure thin film. A clear hexagonal set of diffraction spots is observed. A second set, which has weaker intensity and larger diffraction angle, is also seen. The inset shows a zoom-in image of the area marked with a red square, showing clearly two diffraction spots. The two spots correspond to the electron diffraction from (100) planes of h-BN and graphene, respectively. The calculated inter-planar spacings corresponding to the two spots are 2.13 Å and 2.06 Å, which match well with expected numbers for h-BN and

graphene, respectively. The strong intensity of h-BN diffraction pattern may indicate a well-aligned, multi-layer h-BN. There is a small rotation (<1º) observed between the two sets, similar to other reports on graphene/h-BN heterostructures [36], which also matches our conclusion from Raman spectrum. Figure 2-6 (c) shows a cross-sectional TEM image of the heterostructure. Lattice fringes are observed in the ~15nm thick band. The inter-fringe distance is 0.33nm, which is in close agreement with the out-of-plane lattice constants of h-BN and graphene.

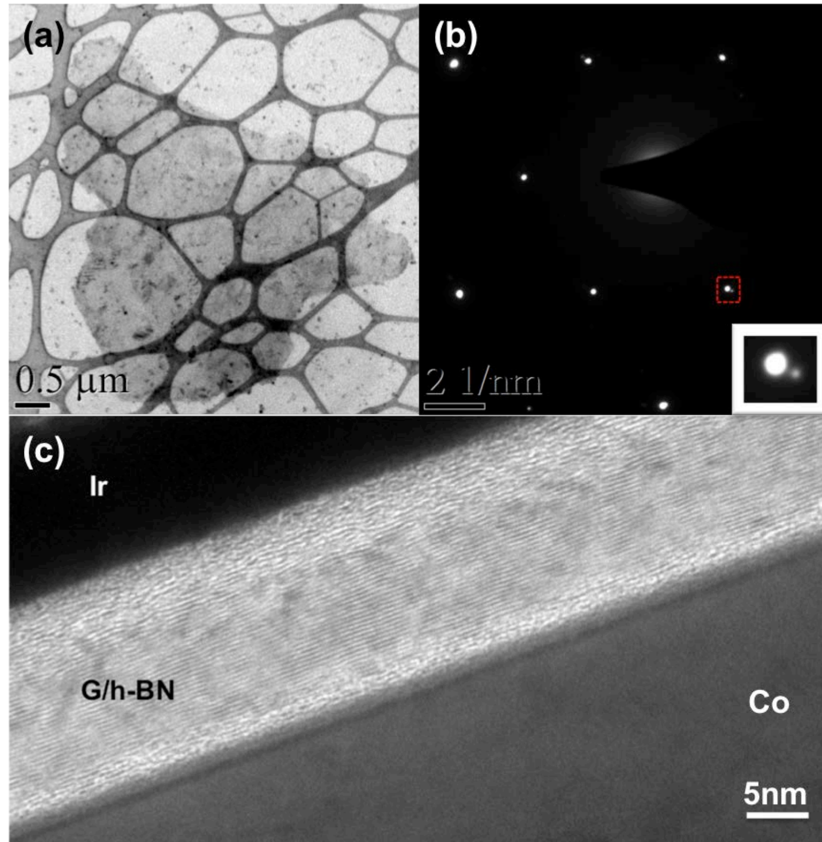

Figure 2-6 (a) Plan-view TEM image of transferred graphene/h-BN heterostructure (Sample B). (b) SAED pattern of Sample B. Diffraction patterns with six-fold symmetry are observed. The inset is enlarged image of the red square area marked in (b). Two diffraction spots are observed, revealing the (100) plane distance of 2.13 Å and 2.06 Å, respectively. (c) Cross-sectional TEM image of Sample B. The thickness of the heterostructure is about 15 nm.

To evaluate the quality of the as-grown graphene film, back-gate MOSFET devices were fabricated based on Sample B after transferred onto SiO_2/Si substrate. Figure 2-7 (a) and (b) shows a schematic and an optical microscopy image of the device. The channel length is 1μm and channel width is 5 μm. Figure 2-7 (c) and (d) show I_D-V_G transfer characteristics and I_D-V_D characteristics of the transistor device, respectively. The mobility is then extracted from the linear regime of the transfer characteristics. For a typical transistor device, its mobility was found to be around 101 $cm^2\ V^{-1}\ s^{-1}$. The present relatively low mobility may mostly originate from the device fabrication process, i.e. the unavoidable residual impurities from the transferring process [37].

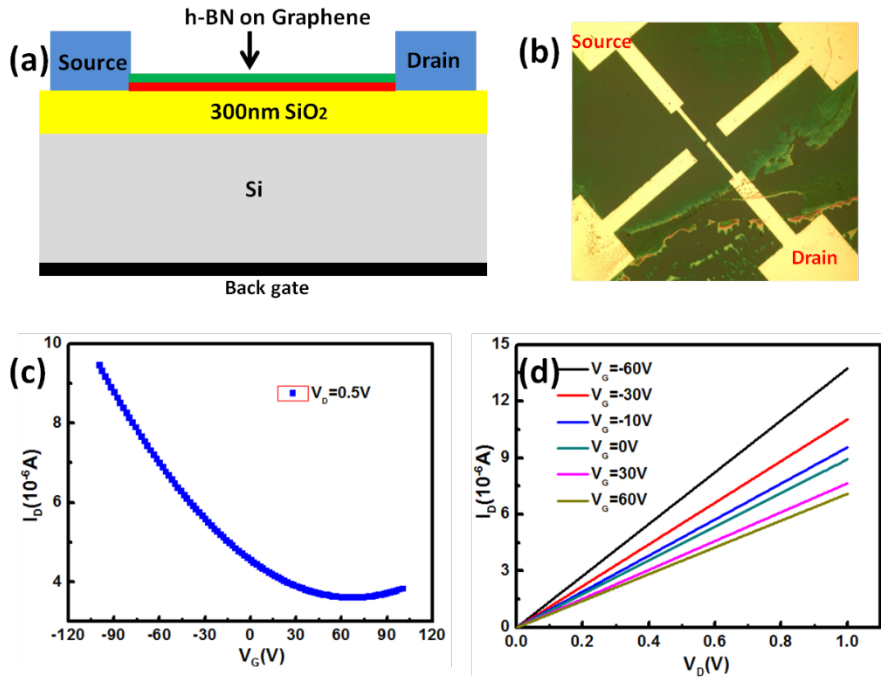

Figure 2-7 (a) Schematic of the transistor device, (b) an optical microscopy image of the transistor device. (c) I_D–V_G characteristics, and (d) I_D-V_D characteristics.

2.4 Summary

In summary, we have demonstrated direct epitaxial growth of h-BN on graphene utilizing MBE. Signature triangular h-BN flakes with sizes as large as 20 μm were observed. Further improvement on the growth condition results in high-quality wafer-scale graphene/h-BN heterostructure single domain film. The epitaxial single/bi-layer graphene/few-layer h-BN structure is further confirmed by XPS, Raman spectroscopy, electron diffraction, and TEM imaging. The misorientation between the graphene and h-BN layers is less than 1°. The successful MBE growth of large-scale graphene/h-BN heterostructure with small mismatch paves a way to greatly improve graphene device performance.

Reference

[1] G. Fiori, F. Bonaccorso, G. Iannaccone, T. Palacios, D. Neumaier, A. Seabaugh, S. K. Banerjee, and L. Colombo, Nat. Nanotechnol. 9, 768-779 (2014).

[2] F. Xia, D. B. Farmer, Y. M. Lin and P. Avouris, Nano Lett. **10,** 715-718 (2010).

[3] K. I. Bolotin, K. J. Sikes, Z. Jiang, M. Klima, G. Fudenberg, J. Hone, P. Kim, and H. L. Stormer, Solid State Commun. **146,** 351–355 (2008).

[4] K. F. Mak, C. Lee, J. Hone, J. Shan and T. F. Heinz, Phys. Rev. Lett. **105,** 136805 (2010).

[5] B. Radisavljevic, A. Radenovic, J. Brivio1, V. Giacometti and A. Kis, Nat. Nanotechnol. **6,** 147–150 (2011).

[6] L. Liu, Y. P. Feng and Z. X. Shen , Phys. Rev. B **68,** 104102 (2002).

[7] K. Watanabe, T. Taniguchi and H. Kanda, Nat. Mat. **3,** 404 – 409 (2004).

[8] R. Mas-Balleste, C. Gomez-Navarro, J. Gomez-Herrero and F. Zamora, Nanoscale **3,** 20-30 (2011).

[9] Q. H. Wang, K. Kalantar-Zadeh, A. Kis, J. N. Coleman and M. S. Strano, Nat. Nanotechnol. **7,** 699–712 (2012).

[10] M. Xu, T. Lian, M. Shi and H. Chen, Chem. Rev. **113,** 3766–3798 (2013).

[11] S. Z. Butler, S. M. Hollen, L. Cao, Y. Cui, J. A. Gupta, H. R. Gutiérrez, T. F. Heinz, S. S. Hong, J. Huang, A. F. Ismach et al., ACS Nano 7, 2898-2926 (2013).

[12] A. K. Geim and I. V. Grigorieva, Nat. **499,** 419-425 (2013).

[13] L. A. Ponomarenko, A. K. Geim, A. A. Zhukov, R. Jalil, S. V. Morozov, K. S. Novoselov, I. V. Grigorieva, E. H. Hill, V. V. Cheianov, V. I. Fal'ko, K. Watanabe, T. Taniguchi, and R. V. Gorbachev, Nat. Phys. **7,** 958–961 (2011).

[14] C. Dean, A. F. Young, L. Wang, I. Meric, G.-H. Lee, K. Watanabe, T. Taniguchi, K. Shepard, P. Kim and J. Hone, Solid State Commun. **152,** 1275–1282 (2012).

[15] T. Georgiou, R. Jalil, B. D. Belle, L. Britnell, R. V. Gorbachev, S. V. Morozov, Y.-J. Kim, A. Gholinia, S. J. Haigh, O. Makarovsky, L. Eaves, L. A. Ponomarenko, A. K. Geim, K. S. Novoselov, and A. Mishchenko, Nat. Nanotechnol. 8, 100-103 (2013).

[16] C. Dean, A. Young, I. Meric, C. Lee, L. Wang, S. Sorgenfrei, K. Watanabe, T. Taniguchi, P. Kim, K. L. Shepard, and J. Hone, Nat. Nanotechnol. 5, 722-726 (2010).

[17] K. Kim, A. Hsu, X. T. Jia, S. M. Kim, Y. M. Shi, M. Dresselhaus, T. Palacios, and J. Kong, ACS Nano 6, 8583–8590 (2012).

[18] G. Giovannetti, P. A. Khomyakov, G. Brocks, P. J. Kelly, J. Brink, Phys. Rev. B **76,** 073103 (2007).

[19] A. F. Young, C. R. Dean, I. Meric, S. Sorgenfrei, H. Ren, K. Watanabe, T. Taniguchi, J. Hone, K. L. Shepard and P. Kim,. Phys. Rev. B **85,** 235458 (2012).

[20] Y. Shi, C. Hamsen, X. Jia, K. Kim, A. Reina, M. Hofmann, A. Hsu, K. Zhang, H. Li, Z. Juang, M. Dresselhaus, L. Li and J. Kong, Nano Lett. 10, 4134-4139 (2010).

[21] C. Bjelkevig, Z. Mi, J. Xiao, P. A. Dowben, L. Wang, W. Mei and J. A Kelber, J. Phys.: Condens. Matter. **22,** 302002 (2010).

[22] Z. Liu, L. Song, S. Zhao, J. Huang, L. Ma, J. Zhang, J. Lou and P. M. Ajayan, Nano Lett. 11, 2032-2037(2011).

[23] W. Yang, G. Chen, Z. Shi, C. Liu, L. Zhang, G. Xie, M. Cheng, D. Wang, R. Yang, D. Shi, K. Watanabe, T. Taniguchi, Y. Yao, Y. Zhang and G. Zhang, Nature mater. 12, 792-797(2013).

[24] A. Koma, K. Sunouchi and T. Miyajima, J. Vac. Sci. Technol. B **3,** 724 (1985).

[25] A. Koma and K. Yoshimura, Thin Solid Films **216,** 72-76 (1992).

[26] N. Zhan, G. Wang and J. Liu, Appl. Phys. A **105,** 341-345 (2011).

[27] J. Park, W. C. Mitchel, L. Grazulis, H. E. Smith, K. G. Eyink, J. J. Boeckl, D. H. Tomich, S. D. Pacley, and J. E. Hoelscher, Adv. Mater. 22, 4140-4145 (2010).

[28] J. M. Garcia, U. Wurstbauer, A. Levy, L. N. Pfeiffer, A. Pinczuk, A. S. Plaut, L. Wang, C. R. Dean, R. Buizza, A. M. Van Der Zande, J. Hone, K. Watanabe, and T. Taniguchi, Solid State Commun. 152, 975-978 (2012).

[29] M. H. Oliveira, Jr., T. Schumann, R. Gargallo-Caballero, F. Fromm, T. Seyller, M. Ramsteiner, A. Trampert, L. Geelhaar, J. M. J. Lopes, and H. Riechert, Carbon 56, 339-350(2013).

[30] N. Zhan, M. Olmedo, G. Wang and J. Liu,Carbon 49, 2046-2052(2011).

[31] X. Li, W. Cai, J. An, S. Kim, J. Nah, D. Yang, R. Piner, A. Velamakanni, I. Jung, E. Tutuc, S. K. Banerjee, L. Colombo, and R. S. Ruoff, Science 324, 1312 (2009).

[32] E. Moreau, F. J. Ferrer, D. Vignaud, S. Godey and S. Wallart, Phys. Status Solidi A **207,** 300-303 (2010).

[33] K. S. Park, D. Y. Lee, K. J. Kim and D. W. Moon, Appl. Phys. Lett. **70**, 315-317(1997).

[34] S. M. Kim, A. Hsu, P. T. Araujo, Y. Lee, T. Palacios, M. Dresselhaus, J.-C. Idrobo, K. Kim and Jing Kong. Nano Lett. **13,** 933-941 (2013).

[35] A. Eckmann, J. Park, H. Yang, D. Elias, A. S. Mayorov, G. Yu, R. Jalil, K. S. Novoselov, R. V. Gorbachev, M. Lazzeri, A. K. Geim and C. Casiraghi, Nano Lett. 13, 5242-5246 (2013).

[36] M. Wang, S. Jang, W.-J. Jang, M. Kim, S.-Y. Park, S.-W. Kim, S.-J. Kahng, J.-Y. Choi, R. Ruoff, Y. Song, and S. Lee, Adv. Mater. 25, 2746-2752 (2013).

[37] O. M. Nayfeh, A. Birdwell, C. Tan, M. Dubey, H. Gullapalli, Z. Liu, A. L. M. Reddy and P. M. Ajayan, Appl. Phys. Lett.102, 103115 (2013)

Chapter 3: Growth of graphene/h-BN heterostructures on Co foil substrate by plasma-assisted MBE

3.1 Introduction

Hexagonal boron nitride (h-BN) is an excellent 2D dielectric layer, and has been studied intensively not only for its exceptional properties but also for its compatibility with graphene (G) and other 2D material systems [1-10]. Recently, much work has been done on the assembly of both lateral and vertical G/h-BN heterostructures [11-21]. Such heterostructures have provided a platform to investigate novel phenomena in fundamental physics such as Hofstadter butterfly effect and quantum Hall effect [22-23], and to develop a variety of nano-devices with superior performance [10, 24-25]. For example, graphene-based transistors using h-BN as a gate insulator and supporting substrate have shown significantly enhanced field-effect carrier mobility in part due to its atomically flat and dangling-bond-free h-BN surfaces, which greatly reduce charge scattering centers at the G/h-BN interfaces [9, 11]. Traditionally, both graphene and h-BN films can be obtained by mechanical exfoliation method and assembled into heterostructures [26]. Although this method can result in crystalline flakes and layered samples, the thickness and size of such samples are difficult to control. On the other hand, chemical vapor deposition (CVD) has been used to provide an alternative approach for the preparation of h-BN/G heterostructures. For example, CVD growth of h-BN (or G) on mechanically

exfoliated G (or h-BN) as well as two-step CVD growth for both G and h-BN have been reported to obtain h-BN and graphene-based heterostructures [11-14, 22]. Although significant progress has been made for these heterostructures, it is still challenging to controllably and scalably synthesize large-area, high-quality layers. MBE is an alternative tool and has natural advantages in high-quality layer-by-layer film deposition thanks to its ultra-high vacuum (UHV) environment, atomic layer epitaxy accuracy and controllability, instant introduction and control of multiple sources, ease of doping of materials and in-situ layer-by-layer characterization. In particular, MBE is promising for the in-situ growth of vertically stacked heterostructures with defect-free interfaces due to the catalytic-free processes since the existing as-grown layers will serve as template for sequential growth [27]. As a matter of fact, the 2D material field is experiencing a surge in using MBE for graphene and BN research, for example, MBE has been used to successfully synthesize graphene and h-BN films on cobalt and nickel thin film substrates [28-32]. More recently, nickel foil has been used to synthesize atomically thin h-BN films by MBE [27]. In this work, we demonstrate the synthesis of h-BN/graphene (h-BN/G) heterostructures on Co foil by sequential deposition of graphene and h-BN layers using plasma-assisted molecular beam epitaxy (MBE). It is found that the coverage of h-BN layers can be readily controlled on the epitaxial graphene by growth time. Large-area, uniform-quality h-BN layers on thin graphite layer were achieved. Based on the h-BN (5-6 nm)/G (26-27 nm) heterostructure, capacitor devices with Co(foil)/G/h-BN/Co(contact) configuration were fabricated to evaluate the dielectric properties of h-BN. The measured breakdown electric field showed a high value of ~2.5-3.2 MV/cm. Both I-V and C-V

characteristics indicate that the epitaxial h-BN film has good insulating characteristics. These results suggest that MBE is a versatile tool to synthesize large-area, uniform-quality h-BN/G heterostructures for the development of high-yield two-dimensional nano-devices.

3.2 Material growth, device fabrication and characterization method

First, cobalt foils (Alfa Aesar, 0.1 mm thick, 99.995%) were cut into 1 cm × 1 cm pieces as substrates. A re-designed Perkin-Elmer MBE system was used for sample growth. A Knudsen effusion cell filled with B_2O_3 powder (Alfa Aesar, 99.999%) was used as boron (B) source. Nitrogen plasma (Airgas, 99.9999%) was generated by an electron cyclotron resonance (ECR) system as nitrogen (N) source. Acetylene gas (Airgas, 99.999%) was used as carbon (C) source.

A Co foil substrate was cleaned with a diluted hydrochloric acid (10%) in order to remove the native oxide layer, rinsed with deionized (DI) water, blown dry and then immediately loaded into the MBE chamber. First, the substrate was heated to 850 ºC and annealed at this temperature under 10-standard cubic centimeters per minute (sccm) flow of hydrogen (H_2) gas for a duration of 20 minutes. Then, the graphene growth started by introducing 3-sccm acetylene (C_2H_2) gas and 6-sccm H_2 gas, and lasted for 60 seconds. Immediately after the graphene growth, h-BN growth started at the same substrate temperature. During the growth, B cell temperature was kept at 1150 ºC, and N_2 gas at a flow rate of 10 sccm through an ECR source along with H_2 gas at a flow rate of 6 sccm were introduced in the chamber. The ECR current was set at 60 mA with a power of 228

W, and the growth took 5, 20 and 30 minutes for three samples, respectively. Finally, the substrate was cooled to room temperature at a rate of 10 ºC/min. A reference sample, i.e., multilayer graphene without h-BN on top was also grown on a Co foil with the same growth condition.

Co(foil)/G/h-BN/Co(contact) capacitor devices were fabricated by standard photolithography and lift-off process. A Co layer of 100 nm was patterned to form top contacts with a size of 250 μm × 250 μm on the surface of as-grown h-BN/G film. Reactive ion etching (RIE) with 50-sccm SF_6 plasma under a power of 50 W was carried out for 15 seconds to etch the h-BN/G film between devices, which ensures isolation of different devices on the same substrate.

Raman characterizations were performed using a HORIBA LabRam system equipped with a 50-mW 514-nm green laser. Scanning electron microscopy (SEM) images were acquired using an XL30-FEG SEM system. X-ray photoelectron spectroscopy (XPS) characterization was carried out using a Kratos AXIS ULTRA XPS system equipped with an Al Kα monochromatic X-ray source and a 165-mm mean radius electron energy hemispherical analyzer. Absorption spectra were measured by a Varian Cary 500 double-beam scanning ultraviolet/visible/near-infrared spectrophotometer. Atomic force microscopy (AFM) images were obtained using a Veeco D3100 AFM system. Transmission electron microscopy (TEM) images were acquired using an FEI/Philips CM-20 TEM**.** Cross-sectional TEM samples were prepared using focused ion beam technique. The h-BN/G thin film was covered first by an amorphous carbon protection layer and further by electron-beam and ion-beam deposited Pt protection

layers. Transferred samples on either SiO_2-coated Si or sapphire substrates were obtained by a PMMA-assisted method. After it was coated with PMMA, the sample was submerged in $FeCl_3$ solution to etch away the Co substrate. The PMMA layer was dissolved in hot acetone (60 ^{o}C) within 12 hours. Current-voltage (I-V) characteristics were obtained by an Agilent 4155C semiconductor parameter analyzer. Capacitance-voltage (C-V) characteristics were obtained by an Agilent 4284A LCR meter.

3.3 Results and discussions

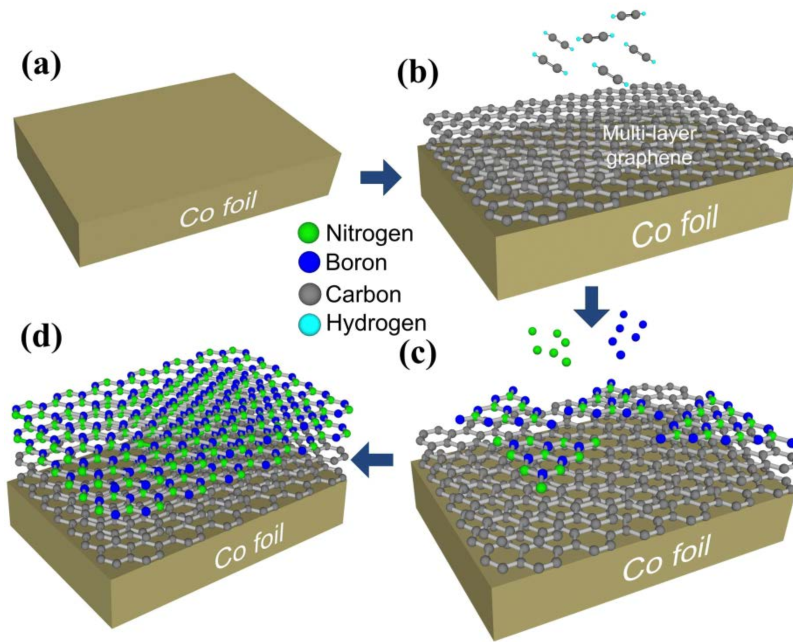

Figure 3-1 Schematic of the growth process of h-BN/G stacked heterostructures. (a) Cleaned Co foil substrate. (b) Layer-by-layer graphene structure grown on fresh Co foil surface. (c) Triangular h-BN domains grown on top of the graphene layers. (d) Connection of triangular h-BN domains to form the first continuous h-BN layer, followed by layer-by-layer growth of h-BN.

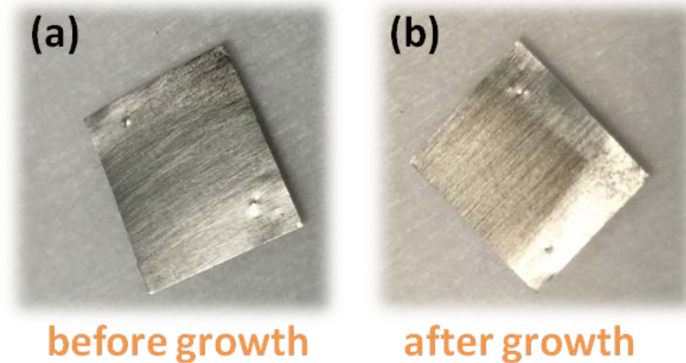

Figure 3-2 Photographs of (a) bare Co foil substrate and (b) as grown h-BN/G sample (Sample D)

Figure 3-1 shows schematic of the growth process of an h-BN/G heterostructure. Figure 3-2 shows photographs of the substrate before and after the growth, indicating the color change as a result of the film growth. Figure 3-3(a) shows an SEM image of as-grown graphene on cobalt foil, i.e., the reference sample (Sample A), presenting a large-scale continuous film. Figure 3-3(b)-(d) show SEM images of as-grown h-BN/G heterostructure samples at an h-BN growth time of 5, 20, 30 minutes for Sample B, C and D, respectively. As seen from Figure 3-3(b) (Sample B), sporadic triangular h-BN flakes have a maximum size of 20 μm and no preferred orientation. This indicates that a short 5-minute growth has already resulted in an evident formation of randomly distributed h-BN seeds on the graphene surface. From theoretical calculations [33], these triangular-shape h-BN domains should end up with a nitrogen-terminated edge due to lower edge energy. At a longer growth duration of 20 minutes (Sample C), the h-BN flakes are increased both in size and density (Figure 3-3(c)). Further increase of h-BN growth time to 30 minutes led to the connection of these h-BN flakes to form a full-coverage continuous film (Sample D), as shown in Figure 3-2(b) and Figure 3-3(d). In addition, much larger h-BN domains with a size of ~40 μm can be observed at the edge area of the sample (inset

of Figure 3-3(d)), which are almost twice the size of the flakes of Sample B (Figure 3-3(b)).

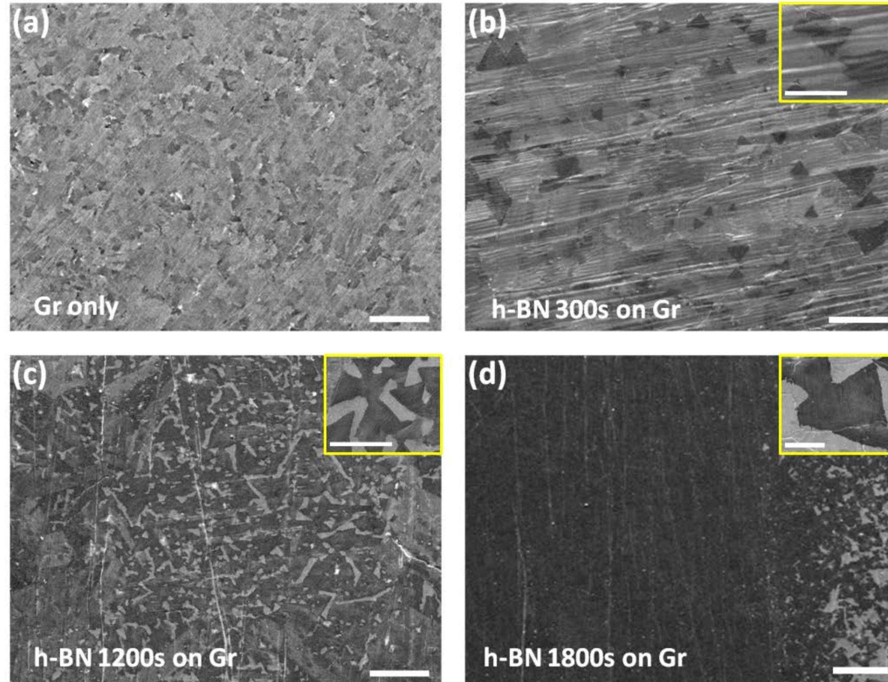

Figure 3-3 SEM image of (a) the graphene (G) on Co foil (Sample A); and h-BN on G film at different h-BN layer growth time: (b) 300 s (Sample B), (c) 1200 s (Sample C), and (d) 1800 s (Sample D). Insets in (b), (c) and (d) are magnified SEM images of local surface areas of these samples. Scale bars in (a-d) are 50 μm. Scale bars for insets in (b-d) are 20 μm.

Figure 3-4 (a) shows Raman spectra of as-grown graphene (Sample A) and h-BN/G heterostructure (Sample D). Both spectra exhibit typical G and 2D peaks of graphene, and the G/2D peak ratio indicates the existence of multilayer graphene. An additional peak is also observed at 1368 cm^{-1} for the h-BN/G sample, corresponding to h-BN E_{2g} optical phonon mode [7]. No graphene D peak can be seen, suggesting that the graphene film has negligible defects [34]. Figure 3-4 (b) shows UV-Vis absorption spectrum, which was measured based on a transferred h-BN/G film on a sapphire substrate. A strong peak at 203 nm and a weak peak at 270 nm are observed in the absorption

spectrum, which are assigned to the optical band gap of h-BN and π-plasmon absorption of graphene, respectively [15-16]. The optical band gap (E_g) value was extracted using the Tauc equation for a direct band gap semiconductor, i.e., $\alpha=C^*(E-E_g)^{1/2}/E$ [5, 35], where α is the absorption coefficient, E is the incident photon energy, and C is a proportionality constant. As shown in Figure 3-4 (c), the E_g of the h-BN film is around 5.85 eV, which matches well with the reported values of few-layer h-BN [2, 4, 7]. The wide band gap also implies the excellent insulating characteristics of as-grown h-BN film. Figure 3-4 (d), (e), and (f) show XPS spectra of C1s, N1s and B1s, respectively. C1s peak at 284.6 eV originates from sp^2 C-C bond [1], representing the existence of graphene. B1s and N1s exhibit energy positions at 190.6 eV and 397.8 eV, respectively, which are consistent with the reported XPS characteristic lines for h-BN [1-4]. Stoichiometry calculation based on the XPS data gives a B/N ratio of 1.08, suggesting an almost equal composition of B and N elements.

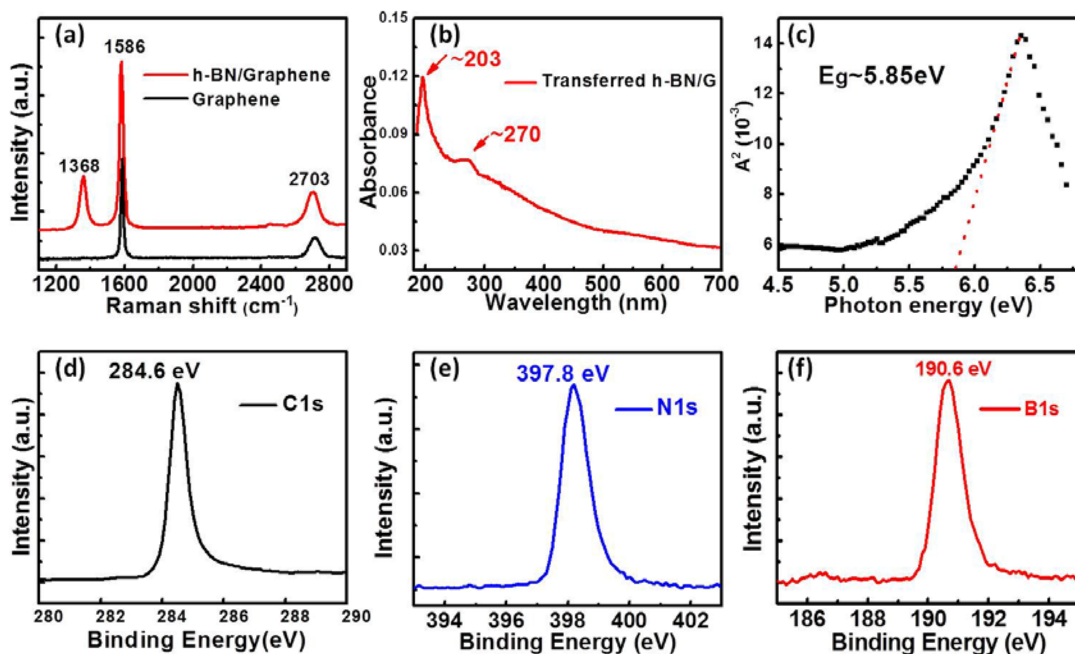

Figure 3-4 (a) Raman spectra of as-grown graphene (Sample A) and h-BN/G heterostructure (Sample D). The G/2D peak ratio in both samples indicates the existence of multilayer graphene. Additional peak is observed besides G and 2D peaks for the h-BN/G sample at 1368 cm^{-1}, corresponding to the E_{2g} optical phonon mode of h-BN. (b) UV-Vis absorption spectrum of a transferred h-BN/G sample on sapphire. (c) α^2 as a function of photon energy. XPS spectra of (d) C1s, (e) N1s, and (f) B1s signals.

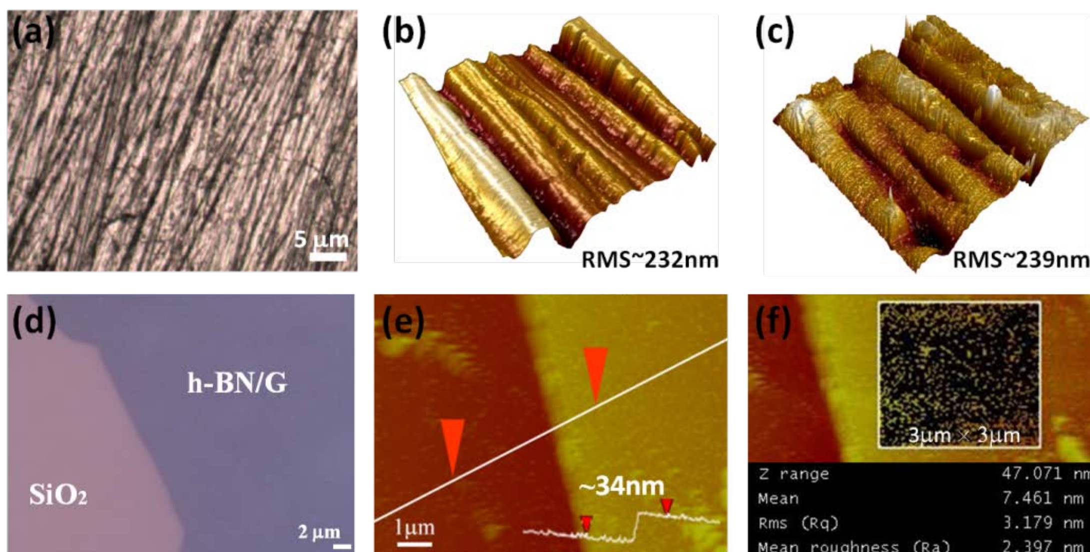

Figure 3-5 (a) Optical microscopy and (b) AFM images of Co foil after high-temperature annealing in vacuum. (c) AFM image of as-grown film, (d) Optical microscopy, and (e-f) AFM images of transferred film of Sample D on SiO_2.

To evaluate the film thickness and morphology, AFM characterization was carried out on a transferred h-BN/G film on SiO_2-coated Si substrate (Figure 3-5). In addition, a Co foil substrate as a reference sample was annealed in the MBE chamber at 850 ºC for 50 minutes under H_2 environment with a flow rate of 10 sccm, which mimics the condition of heat treatment of the substrate of Sample D. Both optical microscopy and AFM images (Figure 3-5(a) and (b), respectively) show the rough surface of cobalt foil substrate. The root mean square (RMS) roughness is around 232 nm within a scan area of 25×25 μm^2. Figure 3-5(c) shows an AFM image of as-grown film (Sample D) on Co foil, which displays a RMS roughness of 239 nm within a scan area of 25×25 μm^2. Figure 3-5(d) shows an optical microscopy image of h-BN/G film of Sample D after transferred on a SiO_2-coated Si substrate. Figure 3-5(e) shows an AFM image of the transferred film, where a scan line indicates the thickness of the h-BN/G film to be 34 nm. Figure 3-5(f) shows an AFM image of a zoomed-in area of 3×3 μm^2, indicating that RMS roughness is around 3.179 nm. Based on the AFM images of h-BN/graphene coated Co foil (Figure 3-5(c)) and bare Co foil (Figure 3-5(b)), it can be concluded that both show similar RMS roughness. In addition, the optical microscopy and AFM images of the transferred h-BN/graphene film show continuous and flat surface. These findings imply that the films were grown conformally across the rough surface.

Figure 3-6(a) shows a cross-sectional TEM image of the h-BN/G heterostructure (Sample D), indicating clear lattice fringes across a total thickness of 32 nm, which is

comparable with the AFM results. The average inter-layer distance was calculated to be 0.348 nm (for total 92 layers), which is in close agreement with the out-of-plane lattice constants of h-BN and/or graphene [25]. To further differentiate the h-BN and G layers, the depth-profile XPS characterization was performed on the as-grown film (Sample D). 2-KeV Ar ion beam was used to sputter a 3×3 mm^2 area with an etching rate of 1 nm per minute. Figure 3-6(b) and (c) show the evolution of N1s, B1s, and C1s XPS peaks during sputtering. As can be clearly seen, the intensities of the N1s and B1s peaks decrease as the sputtering depth increases, indicating that the top h-BN layer was gradually removed by Ar ion beam sputtering. According to Figure 3-6(b), as the sputtering depth reaches ~5-6 nm, N1s and B1s peaks become negligible, which suggests that the top h-BN film has been entirely removed. On the other hand, the C1s peak intensity increases as the sputtering depth increases and saturates beyond the depth of ~5-6 nm. This is consistent with the observed evolution of N1s and B1s peaks. Figure 3-6(d) shows the calculated relative atomic concentration for B, N and C as a function of the sputtering depth. As the sputtering depth increases, both N and B concentrations decrease gradually and reach an insignificant percentage at a sputtering depth of ~5-6 nm, while C concentration gradually levels up and then becomes steady as the etching depths extends from 6 to 20 nm, where the sputtering experiment was stopped. The steady behavior of C1s peak intensity and C concentration can be understood since the thickness of graphene (~27-28 nm) is in fact larger than the total sputtering depth (20 nm). Based on all the above information, it can be concluded that the h-BN/G structure has a top h-BN layer with a thickness of ~5-6 nm and a bottom graphene layer of ~27-28 nm.

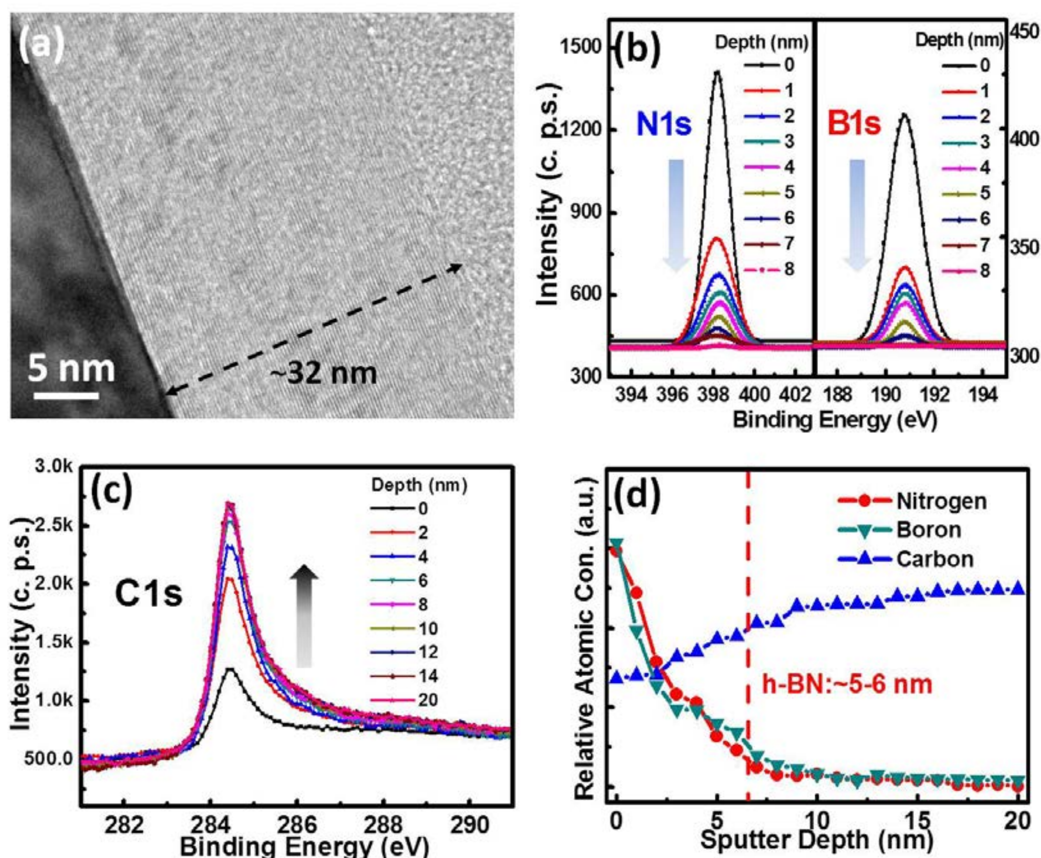

Figure 3-6 (a) Cross-sectional TEM image of as-grown h-BN/G heterostructure on cobalt foil (Sample D). Evolution of (b) N1s, B1s and (c) C1s peaks as a function of sputtering depth in the depth-profile XPS characterization. (d) Relative atomic concentration of B, C and N versus sputtering depth.

In order to evaluate the quality of the h-BN layers, Co(foil)/G/h-BN/Co(contact) capacitor devices were fabricated based on Sample D. The devices with a top Co metal contact of 250 μm × 250 μm are evenly distributed on the sample. Since the devices were directly fabricated on the Co foil substrate rather than based on any transferred h-BN/G films, usual contamination/residues that almost always come with transferring process was truly avoided [6, 24]. Figure 3-7 shows curves of current density (J) versus electric field (E) applied on 20 Co(foil)/G/h-BN/Co(contact) capacitor devices. These curves

exhibit similar behavior, which suggests the film has uniform quality across the sample. As the biases across the capacitors increase, the currents evolve clearly in four regions from fast-increasing region at the beginning, to linearly increasing region under moderate biases, to non-linearly increasing region at higher biases, and finally to sharp-increasing region. These are corresponding to trap-assisted tunneling [24, 36, 37], Ohmic behavior, Fowler-Nordheim tunneling [38], and dielectric breakdown, respectively. By extracting the slope value from the linear portion of the J-E curve in the moderate-bias region, the resistance of 1.16 MΩ can be obtained. Although this value includes contributions from Co/h-BN contact resistance, it implies good insulating characteristics of the h-BN. The breakdown electric field is shown to be ~2.5-3.2 MV/cm in the graph, which is comparable with the observed values from other epitaxial h-BN films [6, 24, 38]. Nevertheless, these fields are slightly lower than that obtained from devices based on exfoliated h-BN films [39]. There are two factors: one is associated with the grain boundaries, wrinkles and pinholes possibly existing in the h-BN films, which can provide leakage paths [24]; the other is related to the rough cobalt foil substrate, whose corrugated surface can induce highly localized electric field by the field enhancement factor [6]. Figure 3-8 shows specific capacitance with the frequency response up to 1 MHz. During the characterization, we calibrated both open-circuit and short-circuit capacitances in order to minimize the impact of the cable capacitance and other noises. As it can be seen from Figure 3-7(b), the specific capacitance decreases as frequency increases. The specific capacitance can be estimated from low-frequency response, i.e., ~4.5 μF/cm^2 (2 kHz). The unit-area capacitances of the devices can be estimated to be 700 nF/cm^2 by

using an ideal parallel-plate capacitor model: $C=\varepsilon_0\times\varepsilon/d$, where ε_0 is vacuum permittivity, ε is relative permittivity of bulk h-BN of 4 [24], and d is h-BN thickness of 5 nm. The measured capacitance is about six times as much as this theoretical value, which should be due to the significant increase in the effective surface area of the rough Co foil substrate, hence, the device has higher charge storage capacity than that of an ideal parallel-plate capacitor. Similar results have been reported that the gully-shape surface can significantly enhance the effective surface area, which serves as tens of thousands of nanoporous or microporous capacitors [40-41].

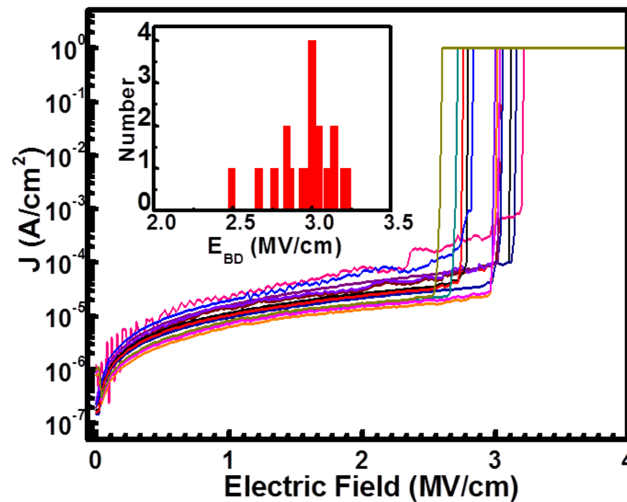

Figure 3-7 Current density versus electric field of 20 Co(foil)/G/h-BN/Co(contact) capacitor devices. All devices have the same size of 250 μm × 250 μm. Inset displays histogram plot of E_{BD}.

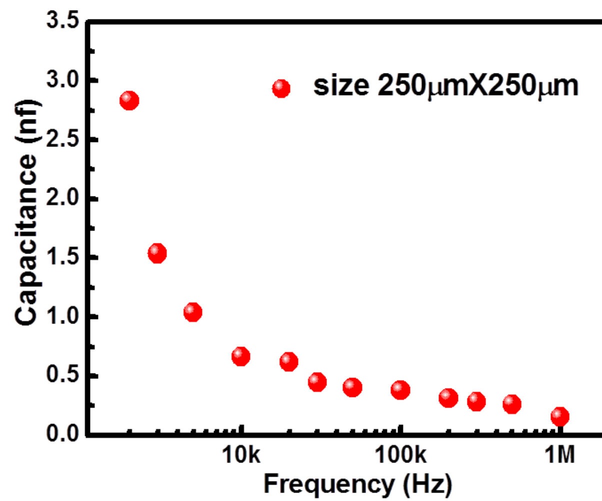

Figure 3-8 Specific capacitance as a function of frequency.

3.4 Summary

In conclusion, we demonstrated the synthesis of stacked h-BN/graphene (h-BN/G) heterostructures on Co foil by sequential deposition of graphene and h-BN through plasma-assisted MBE. Wafer-scale h-BN/G heterostructures consisting multilayer graphene and few-layer h-BN sheets were obtained. Capacitor devices with Co(foil)/G/h-BN/Co(contact) structure were fabricated. Various characterizations including Raman, XPS, AFM, SEM, TEM, UV-Vis absorption, I-V, and C-V were carried out to study the structural, morphological, compositional, resistive, capacitive and dielectric properties of the heterostructures. The breakdown electric field was estimated to be ~2.5-3.2 MV/cm, demonstrating that MBE is an excellent tool for growing high-quality h-BN and G/h-BN heterostructure 2D films.

Reference

[1] L.Song, L. Ci, H. Lu, P. Sorokin, C. Jin, J. Ni, A. Kvashnin, D. Kvashnin, J. Lou, B. Yakobson, and P. Ajayan, Nano Lett. 8, 3209(2010).

[2] Y. Shi, C. Hamsen, X. Jia, K. Kim, A. Reina, M. Hofmann, A. Hsu, K. Zhang, H. Li, Z. Juang, M. Dresselhaus, L. Li, and J. Kong, Nano Lett. 10, 4134(2010).

[3] K. Kim, A. Hsu, X. Jia, S. M. Kim, Y. Shi, M. Hofmann, D. Nezich, J. Rodriguez-Nieva, M. Dresselhaus, T. Palacios, and J. Kong. Nano Lett. 12, 161(2011).

[4] G. Kim, A. R. Jang, H. Y. Jeong, Z. Lee, D. J. Kang, and H. S. Shin, Nano Lett. 13, 1834(2013).

[5] R. Y. Tay, M. H. Griep, G. Mallick, S. H. Tsang, R. S. Singh, T. Tumlin, E. H. T. Teo, and S. P. Karna, Nano Lett. 14, 839(2014).

[6] S. M. Kim, A. Hsu, M. H. Park, S. H. Chae, S. J. Yun, J. S. Lee, D. H. Cho, W. Fang, C. Lee, T. Palacios, M. Dresselhaus, K. K. Kim, Y. H. Lee, and J. Kong, Nat. Commun. 6, 8662(2015).

[7] Y. Gao, W. Ren, T. Ma, Z. Liu, Y. Zhang, W.-B Liu, L.-P. Ma, X. Ma, and H.-M.Cheng, ACS Nano 7, 5199(2013).

[8] P. Sutter, J. Lahiri, P. Zahl, B. Wang, and E. Sutter, Nano lett. 13, 276(2012).

[9] C. Dean, A. Young, I. Meric, C. Lee, L. Wang, S. Sorgenfrei, K. Watanabe, T. Taniguchi, P. Kim, K. L. Shepard, and J. Hone, Nat. Nanotechnol. 5, 722 (2010).

[10]M. P. Levendorf, C. J. Kim, L. Brown, P. Y. Huang, R. W. Havener, D. A. Muller, and J. W. Park, Nature 488, 627(2012).

[11]Z. Liu, L. Song, S. Zhao, J. Huang, L. Ma, J. Zhang, J. Lou, and P. M. Ajayan, Nano. Lett. 11, 2032(2011).

[12]Z. Liu, L. Ma, G. Shi, W. Zhou, Y. Gong, S. Lei, X. Yang, J. Zhang, J. Yu, K. P. Hackenberg, A. Babakhani, J-C. Idrobo, R. Vajtai, J. Lou, and P. M. Ajayan, Nat. Nanotechnol. 8, 119(2013).

[13]T. Gao, X. Song, H. Du, Y. Nie, Y. Chen, Q. Ji, J. Sun, Y. Yang, Y. Zhang, and Z. Liu, Nat. Commun. 6. 6835(2015).

[14]Q. Wu, S. K. Jang, S. Park, S. J. Jung, H. Suh, Y. H. Lee, S. Lee, and Y. J. Song, Nanoscale 7, 7574(2015).

[15]J. H. Meng, X. W. Zhang, H. L. Wang, X. B. Ren, C. H. Jin, Z. G. Yin, X. Liu, and H. Liu, Nanoscale 7, 16046(2015).

[16]C. Zhang, S. Zhao, C. Jin, A. L. Koh, Y. Zhou, W. Xu, Q. Li, Q. Xiong, H. Peng, and Z. Liu, Nat. Commun. 6, 6519(2015).

[17]M. Liu, Y. Li, P. Chen, J. Sun, D. Ma, Q. Li, T. Gao, Y. Gao, Z. Cheng, X. Qiu, Y. Fang, Y. Zhang, and Z. Liu, Nano Lett. 14, 6342(2014)

[18]S. M. Kim, A. Hsu, P. T. Araujo, Y. H. Lee, T. Palacios, M. Dresselhaus, J. C. Idrobo, K. K. Kim, and J. Kong, Nano Lett. 13, 933(2013).

[19]G. H. Han, J. A. Rodriguez-Manzo, C.W. Lee, N. J. Kybert, M. B. Lerner, Z. J. Qi, E. N. Dattoli, A. M. Rappe, M. Drndic, and A. T. C. Johnson, ACS Nano 7, 10129(2013)

[20] L. Liu, J. Park, D. A. Siegel, K. F. McCarty, K. W. Clark, W.Deng, L. Basile, J.Idrobo, A. Li, and G. Gu, Science 343, 163 (2014).

[21] J. M. Garcia, U. Wurstbauer, A. Levy, L. N. Pfeiffer, A. Pinczuk, A. S. Plaut, L. Wang, C. R. Dean, R. Buizza, A. M. Van Der Zande, J. Hone, K. Watanabe, and T. Taniguchi, Solid State Commun. 152, 975 (2012).

[22] W. Yang, G. Chen, Z. Shi, C. Liu, L. Zhang, G. Xie, M. Cheng, D. Wang, R. Yang, D. Shi, K. Watanabe, T. Taniguchi, Y. Yao, Y. Zhang, and G. Zhang, Nature mater. 12, 792(2013).

[23] C. R. Dean, L. Wang, P. Maher, C. Forsythe, F. Ghahari, Y. Gao, J. Katoch, M. Ishigami, P. Moon, M. Koshino, T. Taniguchi, K. Watanabe, K. L. Shepard, J. Hone, and P. Kim, Nature 497, 598 (2013).

[24] K. K. Kim, A. Hsu, X. T. Jia, S. M. Kim, Y. M. Shi, M. Dresselhaus, T. Palacios, and J. Kong, ACS Nano 6, 8583 (2012).

[25] K. K. Kim, A. Hsu, X. Jia, S. M. Kim, Y. Shi, M. Hofmann, D. Nezich, J. F. Rodriguez-Nieva, M. Dresselhaus, T. Palacios, and J. Kong, Nano Lett. 12, 161 (2012)

[26] L. Britnell, R. V. Gorbachev, R. Jalil, B. D. Belle, F. Schedin, A. Mishchenko, T. Georgiou, L. Eaves, S. V. Morozov, N. M. R. Peres, J. Leist, A. K. Geim, K. S. Novoselov, and L. A. Ponomarenko, Science 335, 947 (2012)

[27] S. Nakhaie, J. M. Wofford, T. Schumann, U. Jahn, M. Ramsteiner, M. Hanke, and J. M. J. Lopes, Appl. Phys. Lett. 106, 213108(2015).

[28] N. Zhan, G. Wang, and J. Liu, Appl. Phys. A 105, 341(2011).

[29] Z. Zuo, Z. Xu, R. Zheng, A. Khanaki, J. Zheng, and J. Liu, Sci. Rep., 5, 14760 (2015).

[30] Z. Xu, R. Zheng, A. Khanaki, Z. Zuo, and J. Liu, J. Appl. Phys. Lett. 207, 213103(2015).

[31] A. A. Tonkikh, E. N. Voloshina, P. Werner, H. Blumtritt, B. Senkovskiy, G. Güntherodt, S. S. P. Parkin, and Yu. S. Dedkov. Sci. Rep. 6, 23547 (2016).

[32] H. Ago, Y. Ito, N. Mizuta, K. Yoshida, B. Hu, C. M. Orofeo, M. Tsuji, K. -I. Ikeda, and S. Mizuno, ACS Nano 4, 7407 (2010).

[33] Y. Liu, S. Bhowmick, and B. Yakobson, Nano Lett. 11, 3113(2011).

[34] C. Thomsen, and S. Reich, Phys. Rev. Lett. 85, 5214(2000).

[35] A. Khanaki, H. Abdizadeh, and M. R. Golobostanfard, J. Phys. Chem. C 119, 23250(2015).

[36] Y. Hattori, T. Taniguchi, K. Watanabe, and K. Nagashio, ACS Nano 9, 916(2015).

[37] Y. Ji, C. Pan, M. Zhang, S. Long, X. Lian, F. Miao, F. Hui, Y. Shi, L. Larcher, E. Wu, and M. Lanza. Appl. Phys. Lett. 108, 012905(2016).

[38] G.-H. Lee, Y.-J. Yu, C. Lee, C. Dean, K. L. Shepard, P. Kim, and J. Hone, Appl. Phys. Lett. 99, 243114(2011).

[39] A. F. Young, C. R. Dean, I. Meric, S. Sorgenfrei, H. Ren, K. Watanabe, T. Taniguchi, J. Hone, K. L. Shepard, and P. Kim, Phys. Rev. B, 85, 235458(2012).

[40] N. Guo, J. Q. Wei, Y. Jia, H. H. Sun, Y. H. Wang,K. H. Zhao, X. L. Shi, L. W. Zhang, X. M. Li, A. F. Cao, H. W. Zhu, K. L. Wang, and D. F. Wu, Nano Res. 6, 602(2013).

[41] K. B. Shelimov, D. N. Davydov, and M. Moskovits, Appl. Phys. Lett. 77, 1722(2000).

Chapter 4: Lateral growth of graphene on in situ epitaxial h-BN flakes by plasma-assisted MBE

4.1 Introduction

Layers-structure h-BN currently attract considerable attentions both for its fascinating properties of the individual monolayer and successful incorporation as a complementary two-dimensional dielectric substrate in graphene based electronics from experimental and theoretical work [1-12]. H-BN has a crystal lattice structure similar to that of graphene with less than 2% lattice mismatch [13]. In addition, it is a wide band gap (~5.9 eV) III-V compound with remarkable physical and chemical properties, such as high chemical inertness, high temperature stability, low dielectric constant, large thermal conductivity, and high mechanical strength [4-6]. So far, many methods have been used to obtain atomic h-BN films, such as micromechanical cleavage [14-15], liquid sonication [16] and chemical vapor deposition (CVD) [4-8]. Recently, we have synthesized large single-crystalline h-BN domains and continuous wafer-scale h-BN thin films on epitaxial graphene using plasma-assisted molecular beam epitaxy (MBE) [17]. This result serves as an important first step toward functional nanoelectronic devices based on graphene/h-BN heterostructures. To further enhance processing and integration capability of graphene/h-BN heterostructures for various devices, it is essential to reliably grow graphene on h-BN as well. CVD has already been used to grow single-domain

graphene on exfoliated h-BN [18-19]. Recently, Gao et al reported in-plane and vertically epitaxial growth of graphene on h-BN using benzoic acid precursor on Cu substrate in a CVD system [20]. Nevertheless, direct deposition of high-quality graphene on in situ epitaxial h-BN remains challenging.

In this chapter, we report our results of epitaxial growth of two-dimensional h-BN flakes on Co substrate and growth of wafer-scale graphene on these h-BN flakes using plasma-assisted MBE. Hexagonal boron nitride (h-BN) single-crystal domains were grown on cobalt (Co) substrates at a substrate temperature of 850~900 ^{o}C using plasma-assisted molecular beam epitaxy. Three-point star shape h-BN domains were observed by scanning electron microscopy, and confirmed by Raman and X-ray photoelectron spectroscopy. The h-BN on Co template was used for in situ growth of multilayer graphene, leading to an h-BN/graphene heterostructure. Carbon atoms preferentially nucleate on Co substrate and edges of h-BN and then grow laterally to form continuous graphene. Further introduction of carbon atoms results in layer-by-layer growth of graphene on graphene and lateral growth of graphene on h-BN until it may cover entire h-BN flakes.

4.2 Materials growth and characterization

First, an E-beam evaporation system was used to grow Co film of 400 nm on a 300-nm-thick SiO_2 coated Si (100) substrate. The substrate of 1 cm by 1 cm was cut from the wafer and transferred into an MBE chamber. A Knudsen effusion cell filled with B_2O_3 powder (Alfa Aesar, 99.999%) was used as boron (B) source. A thermocracker was used

to crack acetylene gas (Airgas, 99.999%) as carbon (C) source. An electron cyclotron resonance (ECR) system was used to generate nitrogen plasma (Airgas, 99.9999%) as nitrogen (N) source.

For the growth of h-BN (Sample A), the substrate was firstly annealed at 900 ºC under a hydrogen flow rate of 10 sccm for a duration of 60 minutes. Then, the hydrogen gas flow rate was decreased to 6 sccm, and h-BN was grown at a B cell temperature of 1050 ºC and a nitrogen flow rate of 10 sccm. The ECR current was set at 60 mA with a power of 228 W. The growth lasted for 15 minutes. During the growth of h-BN/graphene stacked layer (Sample B), the h-BN part was grown with a similar growth condition as that of the reference Sample A, except that the substrate temperature was kept at 850 ºC and B cell temperature was 1000 ºC. Graphene was subsequently grown at an acetylene flow rate of 3 sccm through the thermocracker heated at 1200 ºC for 30 seconds. Finally, the substrate was cooled down to room temperature at a rate of 10 ºC/min.

Raman characterizations were performed using a HORIBA LabRam system equipped with a 50-mW 514-nm green laser. Scanning electron microscope (SEM) images were acquired using an XL30-FEG system. X-ray photoelectron spectroscopy (XPS) was carried out using a Kratos AXIS ULTRA XPS system equipped with an Al Kα monochromatic X-ray source and a 165 mm mean radius electron energy hemispherical analyzer. Atomic force microscope (AFM) images were obtained using a Veeco AFM D3100 system.

4.3 Results and discussions

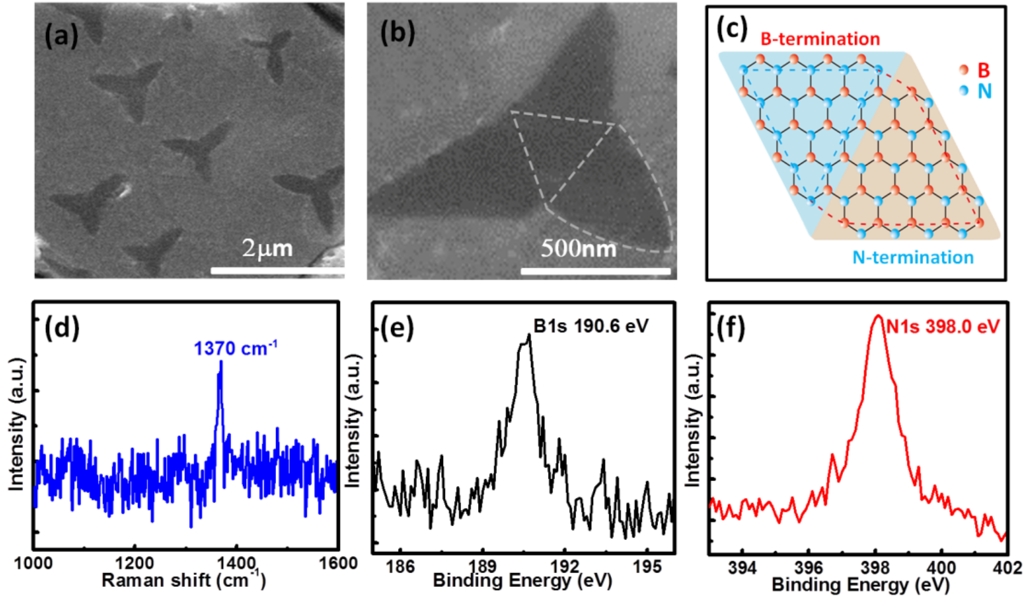

Figure 4-1 (a) SEM image of as grown h-BN domains on Co substrate (Sample A), (b) magnified SEM image of one single h-BN domain, (c) schematic illustration of a possible atom arrangement scheme of the three-point star shape domains. (d) Raman spectrum of Sample A. A peak located at $1370 cm^{-1}$ is observed, relating to E_{2g} optical phonon peak of h-BN, (e) B1s XPS, and (f) N1s XPS spectra of Sample A. B1s peak and N1s peak are at 190.6 eV, and 398.0 eV, respectively, indicating the existence of h-BN.

Figure 4-1(a) shows an SEM image of h-BN sample (Sample A) obtained in secondary electron imaging mode. As seen from the image, three-point star shape h-BN domains of ~1 μm are evident, which are different from the perfect triangular shape of the h-BN domains grown on Cu foil and Ni (111) by CVD [7, 21, 22]. Figure 4-1(b) shows a magnified SEM image of a typical three-point star shape h-BN domain. Each three-point star shape h-BN domain is composed of a central triangle and three sharp triangles at its edge. Visualization of any one of the sharp triangles together with its central triangle, which is marked using dashed lines in the image, gives a “diamond shape” area. Similar results have been also observed for h-BN domains in CVD process [7] and

in other epitaxial two dimensional materials, such as MoS_2 [23] and WS_2 [24]. Figure 4-1(c) shows a schematic of a possible mechanism, which indicates that a nitrogen-terminated triangular shape region connects another boron-terminated triangle back-to-back [7]. From theoretical calculations [21, 25], the nitrogen-terminated triangles have lower edge energy than that of the boron-terminated ones, which suggests that nitrogen-terminated h-BN flakes would be energetically favorable. Therefore, it is likely that the central triangle is boron-terminated while the edges of the three surrounding triangles are nitrogen-terminated. Figure 4-1(d) shows Raman spectrum of Sample A. A Raman peak at 1370 cm^{-1} is observed, which is corresponding to the E_{2g} vibration mode of h-BN and indicates the h-BN film is monolayer [26-28]. Very small full width at half maximum (FWHM) of the peak (15cm^{-1}) suggests that the h-BN is of high quality. Figure 4-1(e) and (f) show XPS spectrum of B1s and N1s state of the sample, respectively. B1s and N1s exhibit an energy position at 190.6 eV and 398.0 eV, respectively, which are typical characteristics of h-BN [5, 29]. Based on the integrated peak intensity, B/N ratio was estimated to be 1:1.03. It means that the compositions of B and N elements are almost equal, indicating that h-BN domains are stoichiometric.

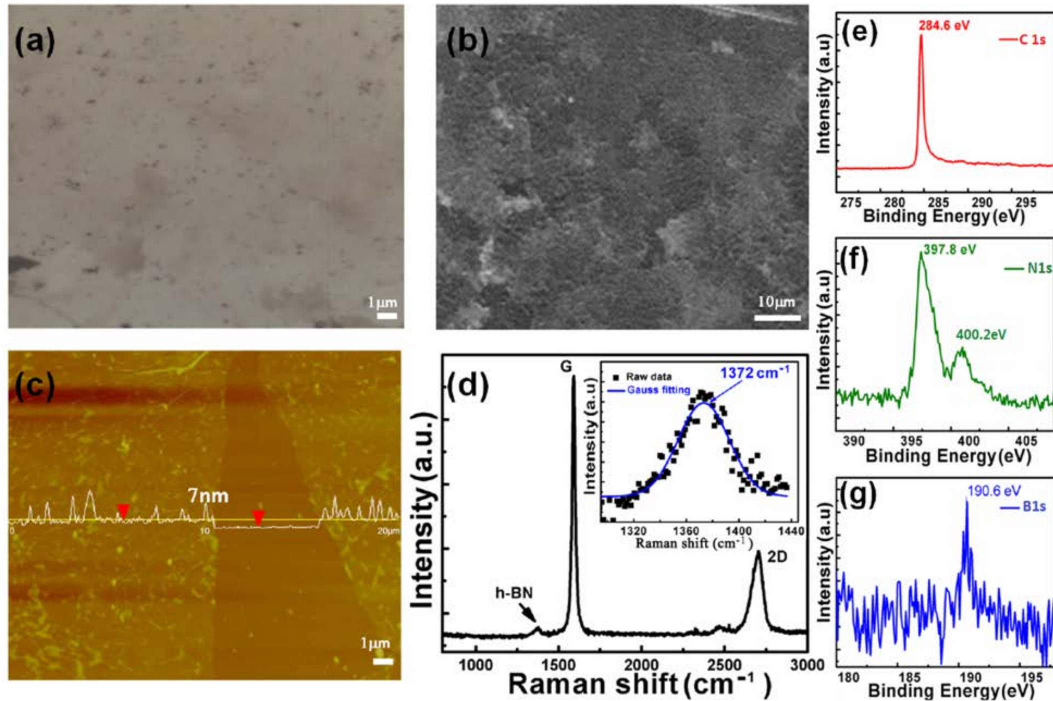

Figure 4-2 (a) Optical microscope image, and (b) SEM image of as grown h-BN/graphene stacked structure (Sample B), (c) AFM image of a transferred h-BN/graphene structure on SiO_2, (d) Raman spectrum of a transferred h-BN/graphene structure on SiO_2. The G/2D peak ratio of graphene indicates the existence of multi-layer graphene. H-BN peak is observed besides G peak. The inset zooms in h-BN peak of 1372 cm^{-1}, relating to E_{2g} optical phonon peak of h-BN, (e), (f), and (g) XPS spectra of C1s, N1s and B1s peaks.

Figure 4-2(a) and (b) show a typical optical microscope image and an SEM image of as grown h-BN/graphene heterostructure (Sample B), respectively. Both images show continuous as grown film, however, color non-uniformity is evident in the images, indicating that the thickness of respective graphene and h-BN layers varies across these imaging areas of the sample. This is a reasonable result from the fact that h-BN is not a continuous film but consists of discrete flakes on the Co substrate. Figure 4-2(c) shows an AFM image of a transferred h-BN/graphene heterostructure, which was transferred onto a SiO_2 substrate using a similar transfer process described in reference [5]. The height profile of a scanned line indicates that the h-BN/graphene has a thickness of ~7

nm on average. Figure 4-2(d) shows Raman spectrum of the transferred sample. The G/2D peak ratio of the graphene signals indicates the existence of multi-layer graphene. An evident peak is also observed at 1372 cm^{-1}, which is corresponding to h-BN E_{2g} optical phonon mode. Moreover, there is no graphene D peak, indicating high-quality graphene film. Figure 4-2 (e), (f), and (g) show XPS spectra of C1s, N1s and B1s, respectively. C1s peak at 284.6 eV originates from sp2 C-C bond [30], which is an indication of the formation of graphene. B1s and N1s exhibit energy positions at 190.6 eV and 397.8 eV, respectively, which are consistent with previous reports of these XPS characteristic lines of h-BN [5, 30]. Moreover, a weak peak at 400.2 eV is observed in Figure 4-2(f), which originates from N-C bonding [31]. The N-C bonding indicates the existence of in-plane hybridization of graphene and h-BN in the heterostructures and further confirms that the h-BN flakes have nitrogen-terminated edges.

Figure 4-3(a) and (b) show Raman mapping result of Sample B for h-BN E_{2g} peak and graphene G peak from one area on the sample, respectively. The insets in (a) and (b) show Raman spectrum of the spots indicated by squares on the image, respectively. It is evident that graphene covers all mapped area, while h-BN Raman signal is found sporadically on the mapped area. It indicates that graphene has grown across these h-BN flakes. Figure 4-3(c) and (d) show Raman mapping result for h-BN E_{2g} peak and graphene G peak on another area on the sample where there is a larger h-BN flake, respectively. As seen from the image in Figure 4-3(c), graphene has not been formed on the h-BN flake. Further careful study of the boundary between the graphene and h-BN leads to an identification of three regions A, B, and C, which are marked on Figure 4-3(d).

Each region manifests its representative Raman spectrum, as shown in the inset. Region A and C show pure h-BN and graphene, respectively, while the boundary region (Region B) exhibits both h-BN and graphene signals.

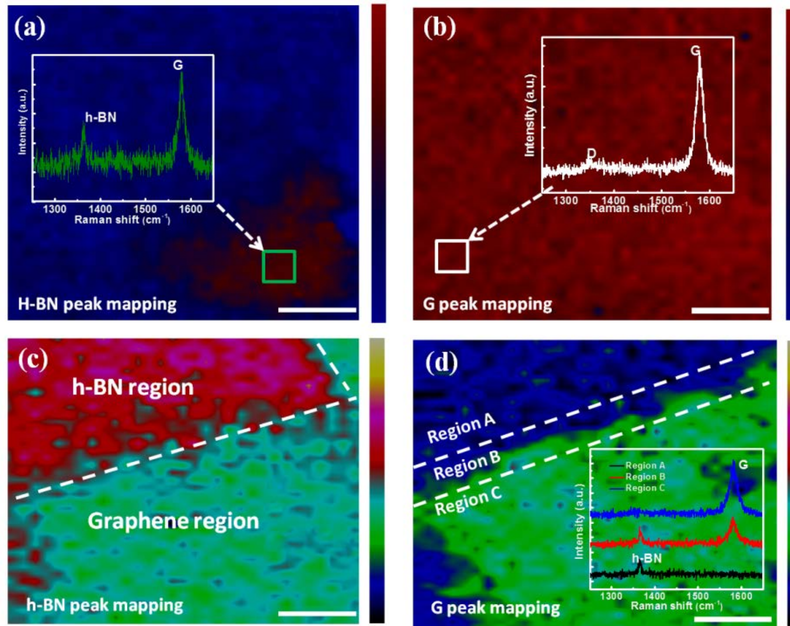

Figure 4-3 Raman mapping of Sample B for a) h-BN E_{2g} peak of h-BN, and b) graphene G peak at one surface area, and c) h-BN E_{2g} peak and d) graphene G peak at another surface area. Insets show Raman spectra accordingly. All scale bars are 1 μm.

Finally we briefly discuss a phenomenological growth mechanism based on the above experimental results, which is schematically shown in Figure 4-4. At the beginning, boron atoms and activated nitrogen atoms impinge on the Co substrate surface to form h-BN flakes (Figure 4-4 (a)). After the growth of h-BN flakes, carbon atoms are introduced and graphene starts to nucleate both on the Co surface [32-33] and at the edges of h-BN flakes [34-35] since these edges serve as perfect atomic steps (Figure 4-4 (b)). The nucleation of graphene on these defect-free surfaces of h-BN flakes is relatively slow. Although the mechanism is still poorly understood, there are experimental findings that

the growth of single-layer graphene on h-BN would take a few hours [17-18, 36]. Then graphene grows laterally to connect each other to form continuous film (Figure 4-4(c)). Further introduction of carbon atoms leads to the layer-by-layer growth of graphene on graphene and further lateral growth of graphene on uncovered h-BN (Figure 4-4(d)). For those small h-BN flakes, graphene can grow across them resulting in h-BN/graphene stacked heterostructures, while for larger flakes, longer graphene growth time is necessary for the entire flakes to be covered. It suggests that the size of h-BN flakes have played a key factor on graphene growth across h-BN flakes.

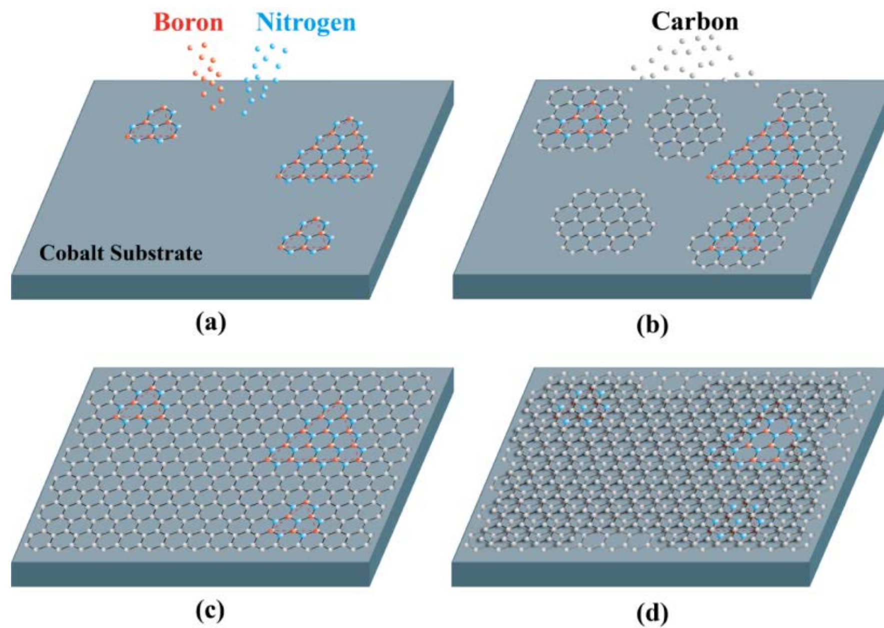

Figure 4-4 Schematic of growth mechanism for the MBE growth of h-BN/graphene heterostructure on Co substrate. a) h-BN nucleation on Co substrate, b) initial graphene nucleation on Co substrate and edges of h-BN flakes, c) lateral growth of graphene, d) layer-by-layer graphene growth on graphene and lateral graphene growth on h-BN flakes.

4.4 Summary

We demonstrated h-BN epitaxial growth on Co substrate by plasma-assisted MBE. Three-point star shape h-BN domains were observed. Based on h-BN growth, we also achieved direct epitaxial growth of h-BN/graphene heterostructures with atomic multi layers. It is found that graphene starts to nucleate on the Co substrate and edges of h-BN flakes, and then grows across h-BN flakes to form local h-BN/graphene heterostructures. Due to negligible nucleation rate of graphene on the surface of h-BN compared with those on the Co substrate and edges of h-BN, larger h-BN flakes are only partially covered by graphene near the edge areas due to lateral graphene growth under a short growth process.

References

[1] Z. Liu, L. Ma, G. Shi, W. Zhou, Y. Gong, S. Lei, X. Yang, J. Zhang, J. Yu, K. P. Hackenberg, A. Babakhani, J-C. Idrobo, R. Vajtai, J. Lou and P. M. Ajayan, Nat. Nanotechnol. 8, 119(2013).

[2] A. Nag, K. Raidongia, R. Datta, K. P. S. S. Hembaram, U. V. Waghmare and C. N. Rao, ACS Nano. 4, 1539(2010).

[3] C. Dean, A. Young, I. Meric, C. Lee, L. Wang, S. Sorgenfrei, K. Watanabe, T. Taniguchi, P. Kim, K. L. Shepard and J. Hone, Nat. Nanotechnol. 5, 722 (2010).

[4] Z. Liu, L. Song, S. Zhao, J. Huang, L. Ma, J. Zhang, J. Lou, and P. M. Ajayan, Nano. Lett. 11, 2032(2011).

[5] L.Song, L. Ci, H. Lu, P. Sorokin, C. Jin, J. Ni, A. Kvashnin, D. Kvashnin, J. Lou, B. Yakobson and P. Ajayan, Nano Lett. 8, 3209(2010).

[6] Y. Shi, C. Hamsen, X. Jia, K. Kim, A. Reina, M. Hofmann, A. Hsu, K. Zhang, H. Li, Z. Juang, M. Dresselhaus, L. Li and J. Kong, Nano Lett. 10, 4134(2010).

[7] K. Kim, A. Hsu, X. Jia, Soo. Kim, Y. Shi, M. Hofmann, D. Nezich, J. Rodriguez-Nieva, M. Dresselhaus, T. Palacios and J. Kong, Nano Lett. 12, 161(2012).

[8] G. Kim, A. Jang, H. Y. Jeong, Z. Lee, D. Kang, and H. Shin, Nano Lett. 13, 1834(2013).

[9] R. Balu, X. Zhong, R. Pandey and S. P. Karna1, Appl. Phys. Lett. 100, 052104(2012).

[10] T. P. Kaloni, Y. C. Cheng, and U. Schwingenschlögl, J. Mater. Chem. 22,919 (2012).

[11] P Moon and M Koshino,Phys. Rev. B 90, 155406 (2014).

[12] A. Principi, M. Carrega, M. B. Lundeberg, A. Woessner, F. H. L. Koppens, G. Vignale and M. Polini, Phys. Rev. B 90, 165408 (2014).

[13] G. Giovannetti, P. Khomyakov, G. Brocks, P. Kelly and J. Brink, Phys. Rev. B 76, 073103(2007).

[14] K. S. Novoselov, D. Jiang, F. Schedin, T. J. Booth, V. V. Khotkevich, S. V. Morozov, and A. K. Geim, Proc. Natl Acad. Sci. 102, 10451(2005).

[15] D. Pacilé, J. C. Meyer, Ç. Ö. Girit, and A. Zettl. Appl. Phys. Lett. 92, 133107(2008).

[16] J. N. Coleman, M. Lotya, A. O'Neill, S. D. Bergin, P. J. King, U. Khan, K.Young, A. Gaucher, S. De, R. J. Smith, I. V. Shvets, S. K. Arora, G. Stanton, H-Y. Kim, K. Lee, G. T. Kim, G. S. Duesberg, T. Hallam, J. J. Boland, J. J. Wang, J. F. Donegan, J. C. Grunlan, G. Moriarty, A. Shmeliov, R. J. Nicholls, J. M. Perkins, E. M. Grieveson, K. Theuwissen, D. W. McComb, P. D. Nellist, and V. Nicolosi, Science 331, 568 (2011).

[17] Z. Zuo, Z. Xu, R. Zheng, A. Khanaki, J. Zheng and J. Liu, Sci. Rep., 5, 14760 (2015).

[18] X. Ding, G. Ding, X. Xie, F. Huang and M. Jiang, Carbon 49, 522(2011).

[19] W. Yang, G. Chen, Z. Shi, C. Liu, L. Zhang, G. Xie, M. Cheng, D. Wang, R. Yang, D. Shi, K. Watanabe, T. Taniguchi, Y. Yao, Y. Zhang and G. Zhang, Nature mater. 12, 792(2013).

[20] T. Gao, X. Song, H. Du, Y. Nie, Y. Chen, Q. Ji, J. Sun, Y. Yang, Y. Zhang and Z. Liu, Nat. Commun. 6. 6835(2015).

[21] W. Auwarter, H. Suter, H. Sachdev and T. Greber, Chem. Mater. 16, 343(2004).

[22] Y. Roland, H. Mark, M. Govind, H. Siu, S. Ram, T. Travis, H. Edwin and P. Shashi, Nano Lett. 14, 839(2014).

[23] A. M. van der Zande, P. Y. Huang, D. A. Chenet, T. C. Berkelbach, Y. You, G. H. Lee, T. F. Heinz, D. R. Reichman, D. A. Muller, J. C. Hone, Nat. Mater., 12, 554(2013)

[24] C. Cong, J. Shang, X. Wu, B. Cao, N. Peimyoo, C. Qiu, L. Sun and T. Yu, Adv. Opt. Mater. 2, 131(2014).

[25] Y. Liu, S. Bhowmick and B. Yakobson, Nano Lett. 11, 3113(2011).

[26] R. Gorbachev, I. Riaz, R. Nair, R. Jali, L. Britnell, B. Belle, E. Hill, K. Novoselov, K. Watanabe, T. Taniguchi, A. Geim and P. Blake, Small 7, 465(2011).

[27] J. Han, J-Y. Lee, H. Kwon and J-S. Yeo, Nanotechnology, 25, 145604(2014).

[28] H. Zhou, J. Zhu, Z. Liu, Z. Yan, X. Fan, J. Lin, G. Wang, Q. Yan, T. Yu, P. Ajayan, and J. M. Tour, Nano Res. 7, 1232 (2014)

[29] K. Park, D. Lee, K. Kim and D. Moon, Appl. Phys. Lett. 70, 315(1997).

[30] E. Moreau, F. Ferrer, D. Vignaud, S. Godey and S. Wallart, Phys. Status Solidi A 207, 300(2010).

[31] C. Zhang, S. Zhao, C. Jin, A. L. Koh, Y. Zhou, W. Xu, Q. Li, Q. Xiong, H. Peng and Z. Liu, Nat. Commun. 6, 6519(2015).

[32] N. Zhan, G. Wang and J. Liu, Appl. Phys. A 105, 341(2011).

[33] E. Kim, H. An, H. Jang, W. Cho, N. Lee, W. Lee, and J. Jung, Chem. Vap. Deposition 17, 9(2011).

[34] L. Liu, J. Park, D. A. Siegel, K. F. McCarty, K. W. Clark, W.Deng, L. Basile, J.Idrobo, A. Li, G. Gu, Science 343, 163 (2014).

[35] M. Liu, Y. Li, P. Chen, J. Sun, D. Ma, Q. Li, T. Gao, Y. Gao, Z. Cheng, X. Qiu, Y. Fang, Y. Zhang, and Z. Liu, Nano Lett. 14, 6342(2014).

[36] J. M. Garcia, U. Wurstbauer, A. Levy, L. N. Pfeiffer, A. Pinczuk, A. S. Plaut, L. Wang, C. R. Dean, R. Buizza, A. M. Van Der Zande, J. Hone, K. Watanabe, and T. Taniguchi, Solid State Commun. 152, 975 (2012).

Chapter 5: Growth of large-area and multi-layer hexagonal boron nitride film on polished Co foils by plasma-assisted MBE

5.1 Introduction

Two-dimensional h-BN film has received a great deal of attention due to its remarkable properties [1-4], such as large band gap, high thermal conductivity, excellent thermal and chemical stability, and its significant potential as an indispensable dielectric layer of building blocks in high-performance 2D integrated electronics and photonics [5-10]. Among those efforts, 2D h-BN, which has a small lattice mismatch (1.7%) with graphene, and an atomically smooth surface that is relatively free of dangling bonds and trapped charges [5], has been recently demonstrated to be an ideal encapsulation for graphene and other 2D materials [8, 11-14]. In addition, h-BN has been used as a gate dielectric to greatly enhance the performance of graphene electronics [5, 15-16]. To realize the technological potential of h-BN, it is essential to synthesize large-area, high-quality h-BN thin films through a scalable and controllable method. So far, tremendous efforts have been made to obtain large-area and high-quality h-BN films. Mechanical cleavage [17] and liquid exfoliation [18] can provide micrometer-sized, atomic-layer-thick h-BN flakes, but they are not suitable for large-area production due to the difficulty of controlling the thickness and size of the materials. Much progress has been made by chemical vapor deposition (CVD) of h-BN growth on various substrates, including Cu [4, 19-21], Ni [22-23], Fe [11, 24], Ru [25] and Pt [26-27]. In addition, other methods, such as physical vapor deposition (pulsed laser deposition [28], reactive magnetron sputtering

[25], ion beam sputtering deposition (IBSD) [21, 29]) and co-segregation [30-31], have been attempted. Nevertheless, there is still much to be done in each one of these methods in order to controllably and scalably synthesize high-quality h-BN thin films.

Most recently, molecular beam epitaxy (MBE) has been used to synthesize h-BN films on Co thin film and nickel (Ni) foil substrates [32-34]. As an alternative approach to other methods, MBE can provide precise control over the growth conditions thanks to its ultra-high vacuum (UHV) environment, atomic layer epitaxy accuracy and controllability, instant introduction and control of multiple sources, ease of doping of materials and in-situ layer-by-layer characterization. In addition, MBE is promising for the in-situ growth of vertically stacked heterostructures with defect-free interfaces [35], which can bring new opportunities to develop integrated 2D nanoelectronics, nanophotonics and spintronics [34]. The growth mechanism is discussed based on the effect of substrate surface morphology on h-BN growth. In this chapter, we report the growth of h-BN films on mechanically polished Co foils using plasma-assisted molecular beam epitaxy for the first time. Under appropriate growth conditions, the coverage of h-BN layers can be readily controlled by growth time. A large-area, multi-layer h-BN film is confirmed by Raman spectroscopy, scanning electron microscopy, X-ray photoelectron spectroscopy and transmission electron microscopy. Dielectric property of as-grown h-BN film is evaluated by characterization of Co(foil)/h-BN/Co(contact) capacitor devices. Breakdown electric field is in the range of 3.0-3.3 MV/cm, which indicates that the epitaxial h-BN film has good insulating characteristics. In addition, the effect of substrate

morphology on h-BN growth is discussed regarding different domain density, lateral size, and thickness of the h-BN films grown on unpolished and polished Co foils.

5.2 Sample preparation and characterization

A re-designed Perkin-Elmer MBE system was used for sample growth. A Knudsen effusion cell filled with B_2O_3 powder (Alfa Aesar, 99.999%) was used as boron (B) source. Nitrogen plasma (Airgas, 99.9999%) generated by an electron cyclotron resonance (ECR) system and high-purity ammonia (American Gas Group, 99.9995%) were used as nitrogen (N) sources. It is worth to mention the reasons that two nitrogen sources were selected in this growth. As is known, N_2 molecules have a strong N-N bond energy, which is very difficult to break up. Although ECR or radio frequency (RF) can be used in exciting the nitrogen molecules into active N atoms or free-radicals, the efficiency of the related growth is quite low in general [36-37]. In addition, there are some reports showing the accelerated ionized nitrogen species would result in structural defects [38]. On the other hand, it is relatively easy to dissociative NH_3, and especially the molecular break-up process can be easily achieved on a heated substrate surface. In addition, hydrogen from decomposition of NH_3 can effectively help remove the oxygen from growth environment. However, using high flux of NH_3 would cause safety issue and high H load for the MBE chamber [39]. Considering all above, the mixture of nitrogen and ammonia as nitrogen sources was selected as a trade-off to minimize the possible negative effects.

Co foils (0.1 mm thick, 99.995%) from Alfa Aesar were cut into 1 cm × 1 cm pieces as substrates. These pieces were degreased with acetone and IPA and rinsed in deionized (DI) water prior to use. Besides these unpolished substrates, polished substrates were mainly used in this experiment. The Co foil surface polishing was performed on an SBT 920 Lapping and Polishing workstation. The Co foil surface polishing was performed on an SBT 920 Lapping and Polishing workstation, as schematically shown in Figure 5-1.

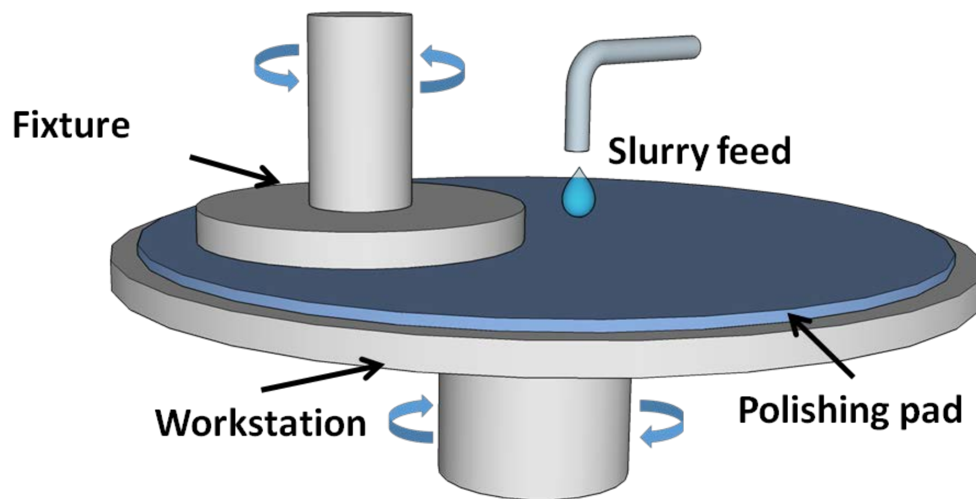

Figure 5-1 Schematic of the polishing machine.

Co foil pieces of 1 cm × 1 cm were mounted on a model 155 lapping and polishing fixture and placed against the workstation. The polishing process was divided into two stages: lapping and polishing. During lapping process, 8-inch abrasive discs of 30, 15, 6 and 3 μm were utilized to remove subsurface damage (scratches and grooves) caused by sawing or grinding, producing a smooth, flat, unpolished surface (generally less than 2.5-μm uniformity). The lapping plate usually rotates at a low speed (<80 rpm). Then, 2-μm silicon oxide powder, 1-μm and 0.3-μm alfa aluminum powder, and 0.06-μm colloidal silica suspension were used sequentially to fine polish Co and produce a scratch-free,

specular surface. Polishing is typically done at very low speeds (<50 rpm) using polishing clothes. After polishing, the polished foil was sonicated by putting in acetone, IPA and DI water, respectively, to remove possible residues. In Figure 5-2, scratched lines are visible on unpolished Co foil while polished Co foil exhibits a shining surface. SEM and EDX have been done to examine the morphology and elemental survey of polished foils, which shows clean and flat surface with the only EDX peak of Co (Figure 5-3).

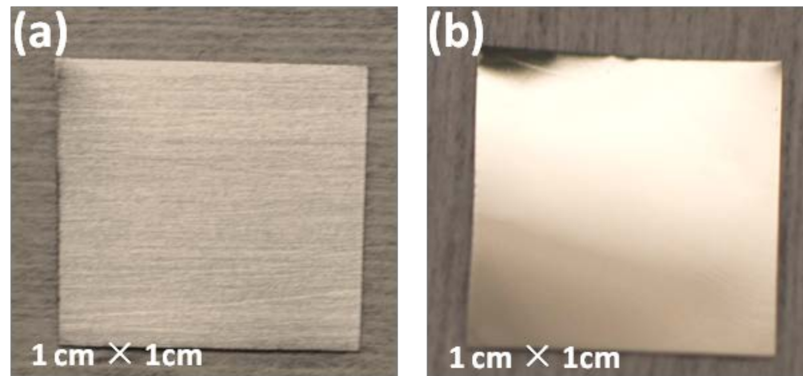

Figure 5-2 Photographs of (a) unpolished Co foil and (b) polished Co foil.

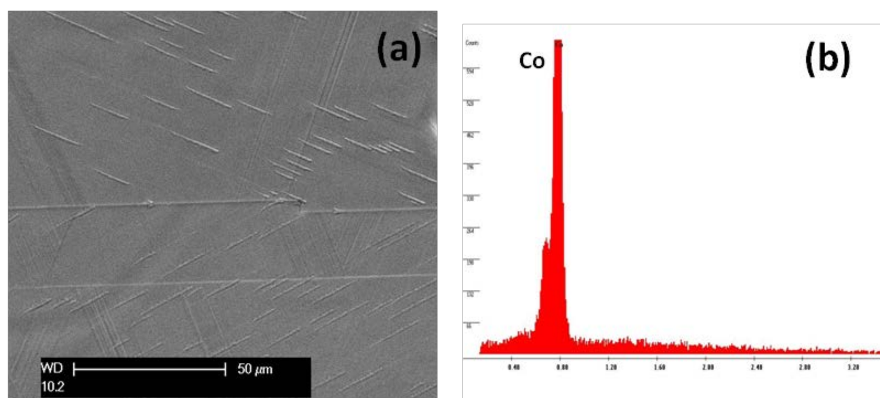

Figure 5-3 (a) SEM image of the polished Co foil and (b) its corresponding EDX spectrum.

These Co foil substrates were cleaned with diluted hydrochloric acid (10%) to remove residual native oxide layer, rinsed with deionized (DI) water, blown dry, and

immediately loaded into the MBE chamber. The substrates were heated to 850 ºC and annealed at this temperature under a 10-sccm (standard cubic centimeters per minute) flow of hydrogen gas for 10 minutes. Then, h-BN growth was started at the same substrate temperature. During the growth, B cell temperature was maintained at 1150 ºC; N_2 gas flowed at 5 sccm through an ECR source, and NH_3 gas at a flow rate of 5 sccm was also introduced to the chamber through a needle valve. The ECR current was set at 60 mA with a power of 228 W, and the growth took 900 s for a reference sample on an unpolished Co foil (Sample A), and 450 s, 900 s and 1800 s on polished Co foils for Samples B, C, and D, respectively. Finally, the samples were cooled to room temperature at a rate of 10 ºC/min. Table 5-1 gives a summary of the growth conditions.

Raman characterizations were performed using a HORIBA LabRam system equipped with a 50-mW, 532-nm green laser. Scanning electron microscopy (SEM) images were acquired using an XL30-FEG SEM system. X-ray photoelectron spectroscopy (XPS) characterization was conducted using a Kratos AXIS ULTRA XPS system equipped with an Al Kα monochromatic X-ray source and a 165-mm mean radius electron energy hemispherical analyzer. Atomic force microscopy (AFM) images were obtained using a Veeco D5000 AFM system. Transmission electron microscopy (TEM) images and selected area electron diffraction (SAED) patterns were acquired using a FEI Tecnai 12 TEM. Plan-view TEM sample was prepared using a PMMA-assisted transfer method. After spin-coating with PMMA, the sample was submerged in $FeCl_3$ solution to etch away the Co metal layer. The film was then transferred onto a carbon-coated Cu TEM grid and treated with acetone and DI water to remove the PMMA. Samples

transferred onto SiO_2-coated Si substrates were obtained using the same PMMA-assisted method.

Step	Parameters	Sample A	Sample B	Sample C	Sample D
Pre-growth Annealing	Temperature	850 °C	850 °C	850 °C	850 °C
	Hydrogen gas flow	10 sccm	10 sccm	10 sccm	10 sccm
	Duration	10 minutes	10 minutes	10 minutes	10 minutes
H-BN Growth	Substrate	*Unpolished Co foil*	*Polished Co foil*	*Polished Co foil*	*Polished Co foil*
	Substrate temperature	850 °C	850 °C	850 °C	850 °C
	Boron cell temperature	1150 °C	1150 °C	1150 °C	1150 °C
	Ammonia gas flow	5 sccm	5 sccm	5 sccm	5 sccm
	Nitrogen gas flow	5 sccm	5 sccm	5 sccm	5 sccm
	Nitrogen ECR current	60 mA	60 mA	60 mA	60 mA
	Growth duration	900 seconds	450 seconds	900 seconds	1800 seconds

Table 5-1 Summary of sample growth condition

Co(foil)/h-BN/Co(contact) capacitor devices were fabricated by a standard photolithography and lift-off process. A Co layer of 100 nm was patterned (square) as top contacts with a lateral size of 20 μm, 50 μm and 100 μm on the surface of as-grown h-BN film. Reactive ion etching (RIE) was performed with a 50-sccm SF_6 plasma, under a power of 50 W, and for 15 seconds to etch the h-BN film between devices, which ensured isolation of different devices on the same substrate. The current-voltage (I-V) characteristics were obtained by an Agilent 4155C semiconductor parameter analyzer

equipped with probing tips having a diameter of 5 μm (Signatone, SE-TL).

5.3 Results and discussion

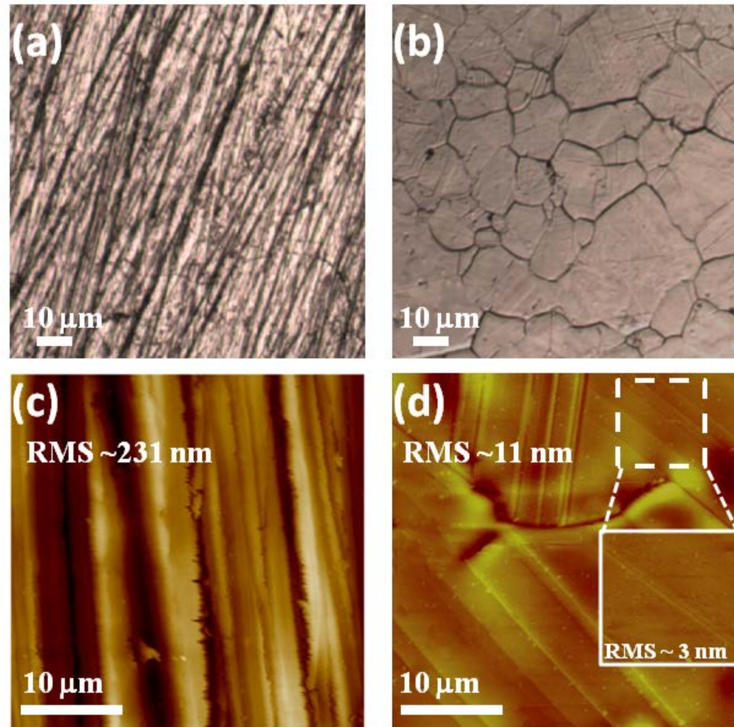

Figure 5-4 Optical microscopy images of (a) unpolished Co foil and (b) polished and high-temperature annealed Co foil. AFM images of (c) unpolished and (d) polished and high-temperature annealed Co foils. The RMS roughness is about 231 nm and 11 nm, respectively. The inset in (d) shows an AFM image of a zoomed-in area with a RMS roughness of ~3 nm.

The surface morphology comparison between unpolished and polished Co foils was characterized by optical microscopy and AFM, and the result is given in Figure 5-4. The rough and deep parallel grooves on the surface of unpolished Co foil can be clearly seen from the optical microscopy and AFM images, as shown in Figure 5-4 (a) and (c), respectively. After mechanical polishing and high-temperature annealing, significant improvement of the surface flatness is evident, as revealed by the optical microscopy and AFM images in Figure 5-4 (b) and (d), respectively. Within a scanned area of 50 × 50

μm^2, the root mean square (RMS) roughness of the polished Co foil is 11 nm, compared to 231 nm for the unpolished Co foil. Moreover, the RMS roughness of selected areas of the polished foil is as small as 3 nm within a scanned area of 10 × 10 μm^2.

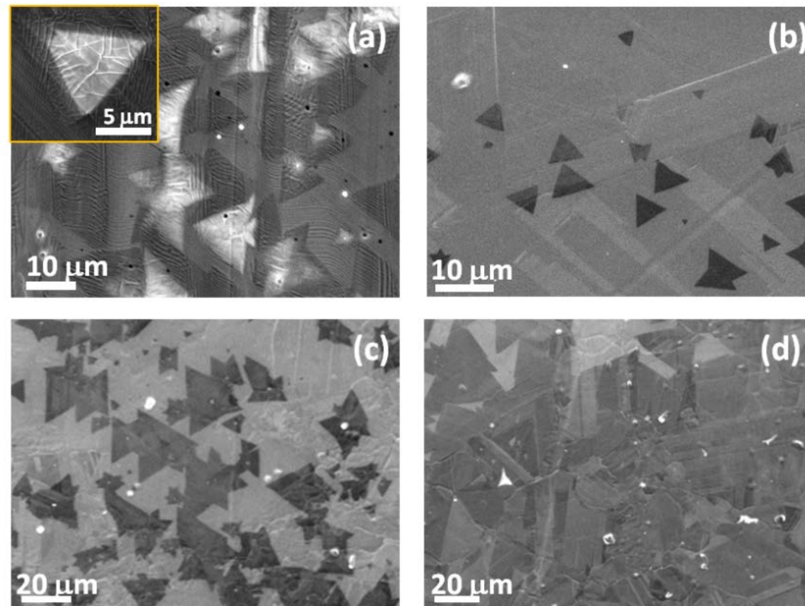

Figure 5-5. SEM images of h-BN films grown on (a) unpolished foil for 900 s (Sample A), and on polished foils for (b) 450 s (Sample B), (c) 900 s (Sample C) and (d) 1800 s (Sample D). The inset in (a) is a magnified image of an h-BN flake on Sample A.

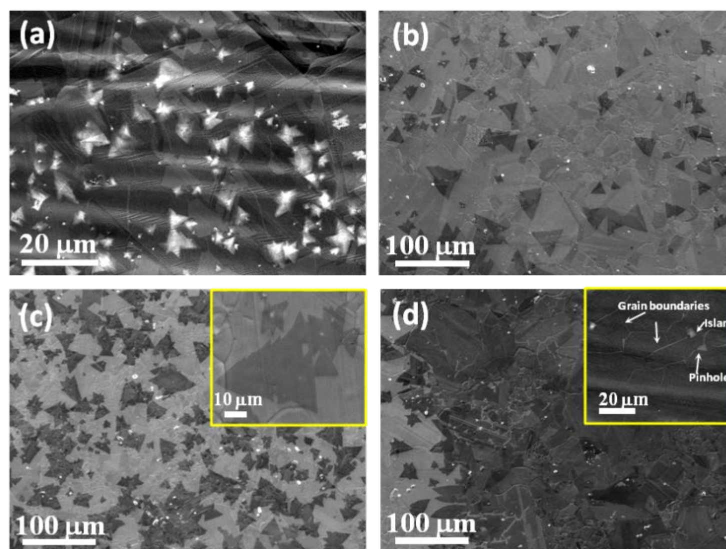

Figure 5-6 Additional SEM images of (a) Sample A, (b) Sample B, (c) Sample C, (d) Sample D. These images were taken with lower magnification compared to those in figure 5-5 in order to show h-BN coverage in larger areas. Insets in (c) and (d) show their corresponding magnified SEM images.

Figure 5-5 (a)-(d) and Figure 5-6 (a)-(d) show SEM images of the four as-grown samples under different magnifications. The contrast between the h-BN films and Co surfaces is clear. White triangular h-BN domains are observed on unpolished Co. The inset of Figure 5-5 (a) shows a magnified SEM image of a typical white triangle which should be multilayer h-BN stacks [21, 24]. This result suggests that the MBE growth of h-BN is not self-limited [21]. As the growth time increases from 450 s to 1800 s, the morphology of h-BN film evolves from discrete flakes into continuous film, as shown in the SEM images in Figure 5-5 (b)-(d). At a growth time of 450 s, Sample B exhibits sparse h-BN flakes in random domain orientations with various edge-sizes from a few micrometers to few tens of micrometers (as large as 40 μm), which indicates the nucleation sites are constantly formed over time, resulting in the earlier seeds grew into larger domains. Longer growth time of 900 s led to denser and relatively larger h-BN flakes, as well as conjoined h-BN domains (Figure 5-6 (c)) on Sample C. However, flakes with smaller sizes can still be seen at this stage, further approving that new seeds have been formed continuously on the exposed Co surface. After the growth is extended to 1800 s, continuous h-BN film is finally formed on most of the Co surface except the edge areas of the sample, where discrete flakes still exist. The single domain boundaries can be easily identified, as indicated in (Figure 5-6 (d)) and the single domain size can be estimated to be in the range of 20-100 um. H-BN flakes growing across Co grain

boundaries are also frequently observed, which suggests that h-BN growth is surface-mediated [19, 21] under these conditions.

Considering the surface morphology effect on the nucleation and growth of h-BN, we compare SEM and AFM images of Sample A (Figure 5-5 (a) and Figure 5-7) and Sample C (Figure 5-5 (c) and Figure 5-8), showing h-BN films on both unpolished and polished Co foils grown under the same growth conditions. In general, the h-BN grown on polished Co foil has larger single-domain size and more uniform thickness, compared with the h-BN grown on unpolished Co foil. It has been proposed that one key approach to grow large, single-crystalline h-BN domains is to reduce the nucleation density at the early stage of growth [20]. The defects, such as grain boundaries, rough edges, uneven grooves, and impurities on unpolished Co substrates provide relatively lower activation energy for h-BN to nucleate compared with smooth regions [40-41]. Since polishing process can remove a large amount of these defects, the nucleation sites are significantly reduced and more evenly distributed on polished Co surfaces. Thus, the h-BN domains grown on polished Co are more uniform in both domain size and thickness, compared with their counterparts on unpolished Co. The low nucleation density decreases the competition for impinging atoms among different seeds locally, which helps maintain the same growth conditions for different seeds. Farther apart seeds grow at the same rate and are evenly spread. After the initial h-BN nucleation, smooth polished Co surface provides lower kinetic energy barrier and longer diffusion length for B and N atoms to diffuse. These atoms with high kinetic energy can diffuse across a large area, and react and settle at the active edges of BN seeds, which continue to grow into large, single-crystalline

domains. In contrast, on unpolished Co surfaces with a larger kinetic energy barrier and lower diffusion length caused by rough surface, B and N atoms tend to accumulate locally and form adlayers, rather than diffuse across the barrier. The formation of adlayers is associated with defects both at the center and edges of existing h-BN layers. In particular, these defects act as nucleation sites and cause more strain at the centers of existing h-BN layers, which favor further nucleation on top of the existing layers [40]. Our result proves that it is indeed important to decrease the number of nucleation sites to achieve large domain sizes. In other words, there is a great possibility to achieve high-quality h-BN films with large-size and single-crystalline domains on smooth Co foil substrates.

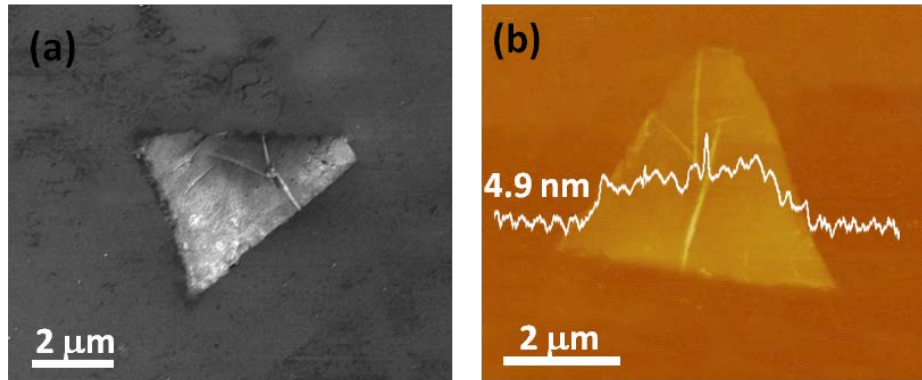

Figure 5-7 SEM (a) and AFM (b) images of an individual h-BN domain from Sample A after transferring on SiO_2/Si substrate. Inset of (b) shows the height profile.

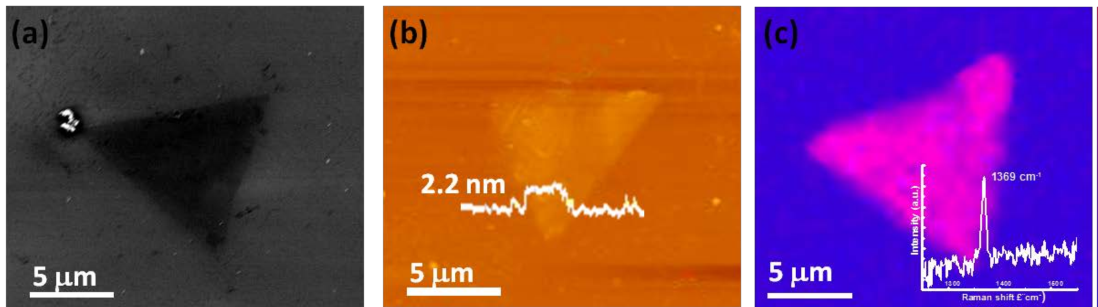

Figure 5-8 SEM (a), AFM (b) and Raman mapping (c) of an individual h-BN domain from Sample C after transferring on SiO_2/Si substrate. Inset of (b) shows the height profile. Inset of (c) is a typical Raman spectrum of transferred h-BN film.

It is interesting to note that besides regular triangular domains, other complex polygons with well-defined edges are observed as the initial form of h-BN flakes among all samples on polished Co substrates. Figure 5-9 (a)-(e) show SEM images of these flakes, and Figure 5-9 (f)-(j) show one-to-one corresponding possible schematic illustrations of their atomic arrangements: triangle shape, “kite” shape, “hourglass” shape, “butterfly” shape and multi-apex-star shape, respectively. From theoretical calculations [42], the triangular h-BN domain is single crystal with nitrogen-terminated zigzag edges due to energetic preferences, as shown in Figure 5-9 (a, f). Figure 5-9 (b, g) show a kite-shape domain composed of two triangles with alternating nitrogen-terminated edges and boron-terminated edges [19]. According to similar consideration to kite-shape domain, hourglass-shape domain is composed of two similar quadrangles with nitrogen-terminated edges and boron-terminated edges, as shown in Figure 5-9 (c, h). In addition, mutually perpendicular edges are observed from butterfly-shape domain (Figure 5-9 (d, i)) and multi-apex-star-shape domain (Figure 5-9 (e, j)), which indicates the connection of one zigzag edge with a neighboring armchair edge from simple geometry. Although the growth mechanism of complex domain structures remains elusive, the two merging modes, namely, point-to-edge and edge-to-edge modes [43] can be a possible explanation. For example, as the nucleation sites are close enough to one another, the coalescence between the domains would occur, resulting in multifaceted shapes.

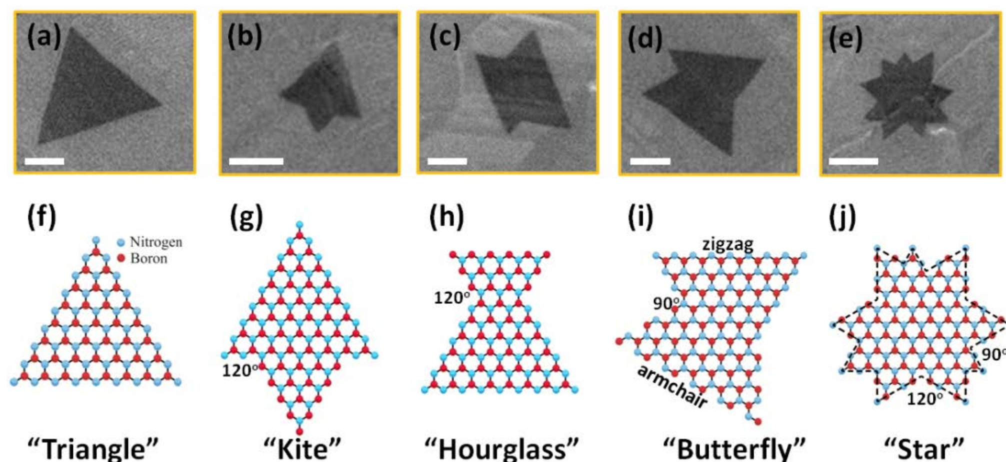

Figure 5-9 SEM images paired with schematic illustrations of h-BN domains with different atomic arrangements: (a, f) triangle shape, (b, g) "kite" shape, (c, h) "hourglass" shape, (d, i) "butterfly" shape and (e, j) multi-apex-star shape. Scale bars in (a)-(e) are 5 μm.

Based on the continuous film of Sample D, further characterizations have been performed to assess the h-BN. Figure 5-10 (a) shows Raman spectrum of as-grown h-BN film. A single peak is observed at 1368 cm^{-1}, which can be assigned to the E_{2g} vibration mode of h-BN [20]. In addition, the full width at half maximum (FWHM) of this Raman peak is only 11 cm^{-1}, which is indicative of high-crystalline h-BN film [33]. XPS spectra in Figure 5-10 (b) and (c) show an evident peak for B 1s and N 1s at 190.6 and 398.0 eV, respectively, further confirming the existence of the B-N bond [4, 11]. The B/N elemental ratio can be extracted as ~1:1.06 based on the integral intensities of the characteristic peaks, which suggests an almost equal composition of B and N elements.

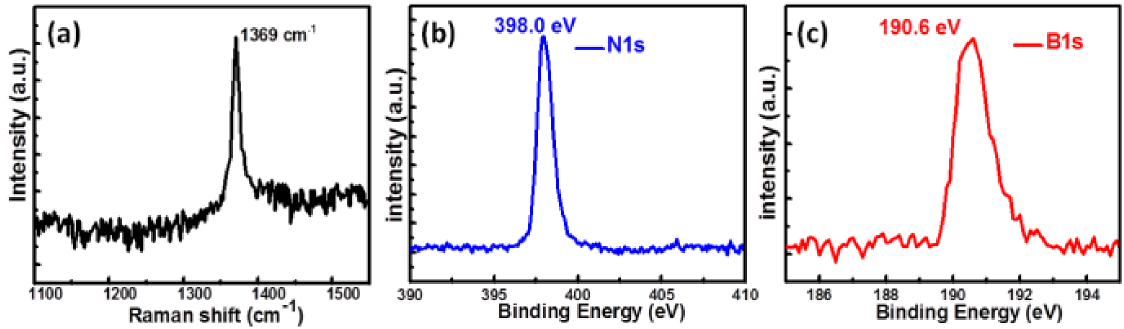

Figure 5-10. (a) Raman spectrum of as-grown h-BN film (Sample D). XPS spectra of (b) N1s and (c) B1s peaks. Current density-electric field characteristics of Co(foil)/h-BN/Co(contact) devices with different contact sizes. Inset shows a schematic of the devices.

Figure 5-11 (a) shows optical microscopy image of the h-BN film transferred onto a SiO_2/Si substrate, showing a large-size continuous film with a clear contrast from the SiO_2/Si substrate. The surface morphology of the h-BN film was further characterized by AFM, which is shown in Figure 5-11 (b). The height profile of a scanned line indicates that the h-BN has a thickness of ~5-6 nm on average for 1800 s growth. It is worth noting that the thickness of h-BN flakes for Sample C (900 s growth) is estimated to be 2.2 nm (Figure 5-8), which suggests the h-BN growth may start with a few layers of nucleation sites and then grow large domains [44]. Comparing the thickness and coverage for Sample C and D, it indicates that, under a longer growth time, the initial flakes grow laterally as well as vertically into multilayer film. Figyre 5-11 (c) shows a plan-view TEM image of the transferred h-BN film. A continuous thin film is observed. The SAED pattern of the h-BN thin film is seen with a clear hexagonal set of diffraction spots. The in-plane lattice constant can be estimated as approximately 2.47-2.5 Å, which is in good agreement with previously reported values of h-BN [22]. High resolution TEM image (Figure 5-11 (d)) shows the lattice fringes of the h-BN film with an interlayer distance of

0.33nm, which matches previous reports of h-BN [11, 31]. The thickness is further measured to be ~ 6 nm, consistent with the AFM results.

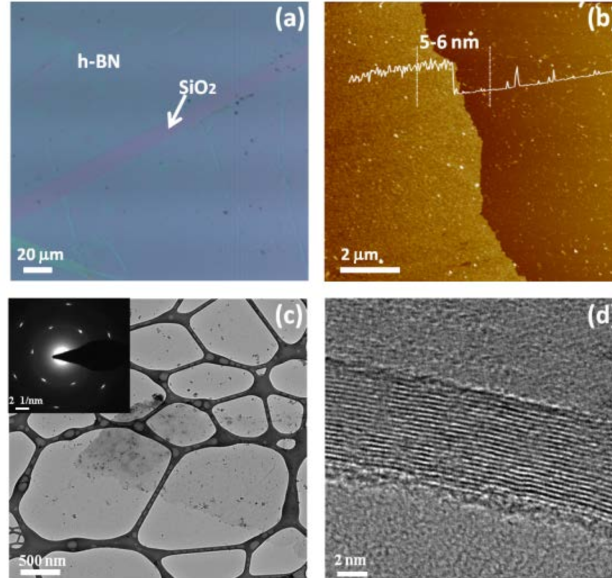

Figure 5-11. (a) Optical micrograph and (b) AFM image of the transferred h-BN film (Sample D) on SiO_2. (c) Plan-view TEM image of the transferred h-BN film on a carbon-coated Cu TEM grid. Inset is an electron diffraction pattern, showing six-fold symmetry of the h-BN film. (d) High-resolution TEM image showing multi-layer structure of the h-BN film near its edge.

To evaluate the film quality, breakdown analysis was performed on Co(foil)/h-BN/Co(metal contact) capacitor device based on Sample D. Figure 5-12 shows the typical curves of current density versus voltage field for different size devices: 100 μm, 50 μm, 20 μm (lateral size of the squared electrode). For the 100 μm size device, it shows significant leakage with no evident breakdown point, which can be originated from the pinholes, grain boundaries or significant defects (Figure 5-6(d)), leading to a conducting behavior. In contrast, devices with 50 μm and 20 μm size show much-improved insulating characteristics although there were still many of the tested devices showing short behavior due to the same factors above mentioned. In addition, it is worth to note

that these smaller size devices has similar leakage current at lower bias compared with those based on mechanically exfoliated BN films [45], the hard breakdown phenomenon can be observed in the range of 3.0-3.3 MV/cm, which is comparable with the values from the devices based on h-BN films grown by CVD [8, 11, 46] and exfoliated h-BN films [47]. In addition to the vertical electrical characterizations, in-plane electrical characterizations were also carried out on a transferred h-BN thin film of Sample D on SiO_2, as shown in Figure 5-13. Currents are negligible under a voltage sweep across pairs of separated metal contacts placed on top of the film. These results suggest good insulating characteristics of the h-BN film grown by MBE.

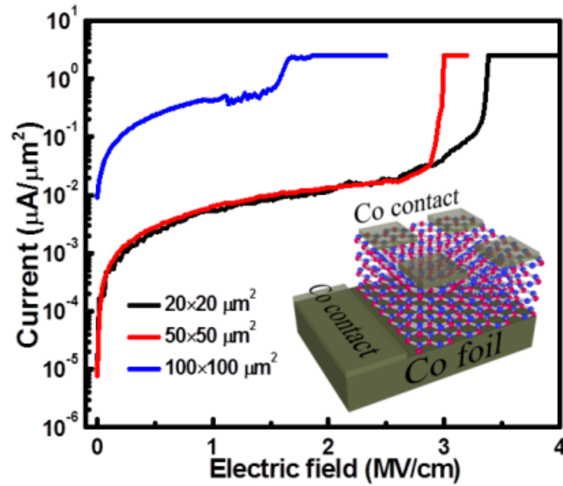

Figure 5-12. Current density-electric field characteristics of Co(foil)/h-BN/Co(contact) devices with different contact sizes. Inset shows a schematic of the devices.

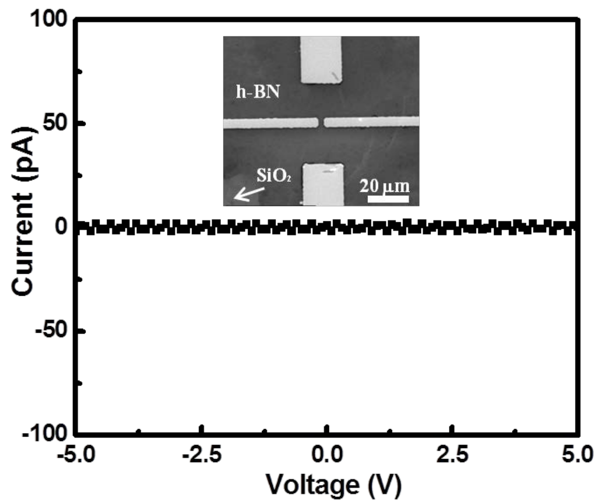

Figure 5-13 Current-voltage characteristic for a transferred h-BN film on SiO_2/Si substrate. The inset shows a SEM image of the devices for two-point probe measurement. The 100 nm Co layers were deposited as top contacts by a standard photolithography and lift-off process. Both devices (horizontal and vertical) show almost no current flow through the devices in the scanned range of voltage (-5/+5), indicating the insulating nature of h-BN.

5.4 Summary

In conclusion, we demonstrated large area growth of multi-layer h-BN films on mechanically polished Co foils using plasma-assisted MBE. Time-dependent h-BN growth indicates that the coverage of h-BN domains with various polygon shapes on the surface increases as the increase of the growth time. The dielectric properties of as-grown h-BN film are evaluated by characterization of Co(foil)/h-BN/Co(contact) capacitor devices. Breakdown electric field is estimated to be 3.0-3.3 MV/cm, which indicates that the epitaxial h-BN film has good insulating characteristics. In addition, by comparing the results of h-BN growth on unpolished and polished Co foils, it is concluded that the morphology of Co foil surface affects h-BN growth with respect to domain density,

lateral size and thickness since the control of the density of nucleation sites plays a key role toward the growth of h-BN films.

REFERENCES

[1] A. Nag, K. Raidongia, R. Datta, K. P. S. S. Hembaram, U.V. Waghmare and C. N. R. Rao, ACS Nano 2010, 4, 1539-1544(2010).

[2] L. Liu, Y. P. Feng and Z. X. Shen, Rev. B 68, 104102(2003).

[3] K. Watanabe, T. Taniguchi and H. Kanda, Nat. Mat. 3, 404-409(2004).

[4] L.Song, L. Ci, H. Lu, P. Sorokin, C. Jin, J. Ni, A. Kvashnin, D. Kvashnin, J. Lou, B. Yakobson and P. Ajayan, Nano Lett. 8, 3209-3215(2010).

[5] C. Dean, A. Young, I. Meric, C. Lee, L. Wang, S. Sorgenfrei, K. Watanabe, T. Taniguchi, P. Kim, K. L. Shepard, and J. Hone, Nat. Nanotechnol. 5, 722-726 (2010).

[6] M. P. Levendorf, C. J. Kim, L. Brown, P. Y. Huang, R. W. Havener, D. A. Muller and J. W. Park, Nature 488, 627-632(2012).

[7] C. R. Dean, L.Wang, P. Maher, C. Forsythe, F. Ghahari, Y. Gao, J. Katoch, M. Ishigami, P. Moon, M. Koshino, T. Taniguchi, K. Watanabe, K. Shepard, J. Hone, and P. Kim, Nature, 497, 598-602(2013).

[8] K. K. Kim, A. Hsu, X. Jia, S. M. Kim, Y. Shi, M. Dresselhaus, T. Palacios and J. Kong, J. ACS Nano 6, 8583-8590(2012).

[9] K. H. Lee, H. J. Shin, J. Lee, I. Y. Lee, G. H. Kim, J. Y. Choi and S. W. Kim, Nano Lett. 12, 714-718(2012).

[10] L. Britnell, R. Gorbachev, R. Jalil, B. Belle, F. Schedin, A. Mishchenko, T. Georgiou, M. Katsnelson, L. Eaves, S. Morozov, N. Peres, J. Leist, A. Geim, K. Novoselov and L. Ponomaremko, Science 2012, 335, 947-950(2012).

[11] S. M. Kim, A. Hsu, M. H. Park, S. H. Chae, S. J. Yun, J. S. Lee, D. H. Cho, W. Fang, C. Lee, T. Palacios, M. Dresselhaus, K. K. Kim, Y. H. Lee, and J. Kong, Nat. Commun. 6, 8662(2015)

[12] A. Yan, J. Velasco Jr, S. Kahn, K. Watanabe, T. Taniguchi, F. Wang, M. Crommie and A. Zettl, Nano Lett. 15(10), 6324-6331(2015).

[13] S. Wang, X. Wang and J. Warner, ACS Nano 9, 5246-5254(2015).

[14] M. Okada, T. Sawazaki, K. Watanabe, T. Taniguch, H. Hibino, H. Shinohara and R. Kitaura, ACS Nano 8, 8273-8277(2014).

[15] L. Britnell, R. Gorbachev, R. Jalil, B. Belle, F. Schedin, A. Mishchenko, T. Georgiou, M. Katsnelson, L. Eaves and S. Morozov, Science 335, 947-950(2012).

[16] L. Wang, B. Wu, J. Chen, H. Liu, P. Hu and Y. Liu, Adv. Mater. 26, 1559-1564(2014).

[17] K. S. Novoselov, D. Jiang, F. Schedin, T. Booth, V. V. Khotkevich, S. V. Morozov, and A. K. Geim, Proc. Natl. Acad. Sci. U.S.A. 102, 10451-10453(2005).

[18] J. N. Coleman, M. Lotya, A. O'Neill, S. D. Bergin, P. J. King, U. K. Young, A. Gaucher, S. De, R. J. Smith, I. V. Shvets et al., Science 331, 568-571(2011).

[19] K. K. Kim, A. Hsu, X. Jia, S. M. Kim, Y. Shi, M. Hofmann, D. Nezich, J. F. Rodriguez-Nieva, M. Dresselhaus, T. Palacios and J. Kong, Nano Lett. 12, 161-166(2011).

[20] R. Y. Tay, M. H. Griep, G. Mallick, S. H. Tsang, R. S. Singh, T. Tumlin, E. H. T. Teo, and S. P. Karna, Nano Lett. 14, 839- 846(2014).

[21] H. Wang, X. Zhang, J. Meng, Z. Yin, X. Liu, Y. Zhao and L. Zhang, Small 11, 1542-1547(2015).

[22] Y. Shi, C. Hamsen, X. Jia, K. Kim, A. Reina, M. Hofmann, A. Hsu, K. Zhang, H. Li, Z. Juang, M. Dresselhaus, L. Li, and J. Kong, Nano Lett. 10, 4134-4139(2010).

[23] A. Ismach, H. Chou, D. A. Ferrer, Y. Wu, S. McDonnell, H. C. Floresca, A. Covacevich, C. Pope, R. Piner, M. J. Kim, R. M. Wallace, L. Colombo and R. S. Ruoff, ACS Nano 6, 6378-6385(2012).

[24] S. Caneva, R. Weatherup, B. Bayer, R. Blume, A. Cabrero-Vilatela, P. Braeuninger-Weimer, M. Martin, R. Wang, C. Baehtz, R. Schloegl and J. Meyer, Nano Lett. 16, 1250-1261(2016).

[25] P. Sutter, J. Lahiri, P. Zahl, B. Wang and E. Sutter, Nano Lett. 13, 276-281(2012).

[26] G. Kim, A. Jang, H. Jeong, Z. Lee, D. Kang and H. Shin, Nano Lett. 13, 1834-1839(2013).

[27] Y. Gao, W. Ren, T. Ma, Z. Liu, Y. Zhang, W. Liu, L. Ma, X. Ma and H. Cheng, ACS Nano 7, 5199-5206(2013).

[28] N. R. Glavin, M. L. Jespersen, M. H. Check, J. Hu, A. M. Hilton, T. S. Fisher and A. A. Voevodin, Thin Solid Films 572, 6-11(2014).

[29] J. H. Meng, X. W. Zhang, H. L. Wang, X. B. Ren, C. H. Jin, Z. G. Yin, X. Liu and H. Liu, Nanoscale 7, 16046-16053(2015).

[30] C. Zhang, S. Zhao, C. Jin, A. Koh, Y. Zhou, W. Xu, Q. Li, Q. Xiong, H. Peng, and Z. Liu, Nat. Commun. 6, 6519(2015).

[31] C. Zhang, L. Fu, S. Zhao, Y. Zhou, H. Peng and Z. Liu, Adv. Mater. 26, 1776-1781(2014).

[32] Z. Xu, R. Zheng, A. Khanaki, Z. Zuo and J. Liu, Appl. Phys. Lett. 207, 213103(2015).

[33] S. Nakhaie, J. M. Wofford, T. Schumann, U. Jahn, M. Ramsteiner, M. Hanke, J. M. J. Lopes and H. Riechert, Appl. Phys. Lett. 106, 213108(2015).

[34] A. A. Tonkikh, E. N. Voloshina, P. Werner, H. Blumtritt, B. Senkovskiy, G. Güntherodt, S. S. P. Parkin and Y. S. Dedkov ,Sci. Reps. 6, 23547(2016).

[35] Z. Zuo, Z. Xu, R. Zheng, A. Khanaki, J. Zheng and J. Liu, Sci. Rep. 5, 14760(2015).

[36] M. J. Paisley, Z. Sitar, Benda Van and R. F. Davis, J. Vac. Sci. Technol. B 8, 323-326(1990).

[37] C. L. Tsai,Y. Kobayashi,T. Akasaka and M.Kasu, J. Cryst. Growth 311, 3054-3057(2009).

[38] V. A. Grant, R. P. Campion, C. T. Foxon, W. Lu, S. Chao and E. C. Larkins, Semicond. Sci. Technol. 22, 15-19(2007).

[39] C. Skierbiszewski, Z. R. Wasilewski, I. Grzegory, and S. Porowski, J. Cryst. Growth 311, 1632-1639(2009)

[40] M. H. Khan, Z. Huang, F. Xiao, G. Casillas, Z. Chen, P. J. Molino and H. K. Liu, Sci. Rep. 5, 7743(2015).

[41] R. Y. Tay, M. H. Griep, G. Mallick, S. H. Tsang, R. S. Singh, T. Tumlin, E. H. T. Teo and S. P. Karna, Nano Lett. 14, 839- 846(2014).

[42] Y. Liu, S. Bhowmick, B. Yakobson, Nano Lett. 11, 3113-3116(2011).

[43] L. Wang, B. Wu, L. Jiang, J. Chen, Y. Li, W. Guo, P. Hu and Y. Liu, Adv. Mater. 27, 4858-4864(2015).

[44] R. Y. Tay, X. Wang, S. H. Tsang, G. C. Loh, R. S. Singh, H. Li, G. Mallick and E. H. T. A. Teo, J. Mater. Chem. C 2, 1650-1657(2014).

[45] L. Britnell, R. V. Gorbachev, R. Jalil, B. D. Belle, F. Schedin, M. I. Katsnelson, L. Eaves, S. V. Morozov, A. S. Mayorov, N. M. R. Peres, A. H. C. Neto, J. Leist, A. K. Geim, L. A. Ponomarenko, and K. S. Novoselov, Nano Lett. 12, 1707-1710(2012).

[46] M. S. Bresnehan, G. R. Bhimanapati, K. Wang, D. W. Snyder and J. A. Robinson, ACS Appl. Mater. Interfaces, 6, 16755-16762(2014).

[47] G.-H. Lee, Y.-J. Yu, C. Lee, C. Dean, K. L. Shepard, P. Kim and J. Hone, Appl. Phys. Lett. 99, 243114(2011).

Chapter 6: Summary

Graphene and h-BN, as promising 2D materials have been studied intensively to prepare for the next generation nano-electronics. To realize the technological potential of 2D system, it is essential to synthesize large-area, high-quality 2D thin films through a scalable and controllable method. In this dissertation, the growth of graphene, h-BN and their vertical and lateral heterostructures by MBE is mainly investigated, and the growth mechanism, fundamental physics and possible applications are also discussed.

In chapter 2, in-situ epitaxial growth of graphene/h-BN heterostructures on Co film substrate was achieved by using plasma-assisted MBE. The direct Graphene/h-BN vertical stacking structures were demonstrated and further confirmed by various characterizations, such as Raman spectroscopy, SEM, XPS and TEM. Large area heterostructures consisting of single-layer/bilayer graphene and multilayer h-BN were achieved. The mismatch angle between graphene and h-BN is below 1°.

In chapter 3, the growth of graphene-h-BN capacitor structures on Co foil substrate by plasma-assisted MBE is discussed. It is found that the coverage of h-BN layers on the epitaxial graphene is growth-time dependent. Wafer-scale, uniform-thickness h-BN heterostructures were successfully deposited on multilayer graphene. Capacitor devices with Co(foil)/G/h-BN/Co(contact) configuration were fabricated to evaluate the dielectric properties of h-BN. The measured breakdown electric field showed a high value of 2.5-3.2 MV/cm. Both I-V and C-V characteristics indicated that the epitaxial h-BN film is of insulating characteristics.

In chapter 4, the lateral growth of graphene on in situ epitaxial h-BN flakes by plasma-assisted MBE was studied. Single-crystal h-BN domains were grown on Co film substrates at a substrate temperature of 850~900 ^{o}C. Three-point star shape h-BN domains were observed by SEM, and the B-N bonds were confirmed by Raman and XPS. In addition, the lateral growth mechanism is discussed. The h-BN flakes on Co surface can be a template used for sequential growth of multilayer graphene, leading to an h-BN/graphene heterostructure.

In chapter 5, it mainly studied the growth of large-area and high-quality h-BN atomic layers on polished Co foils by plasma-assisted MBE. The coverage of h-BN layers can be readily controlled by growth time under appropriate growth conditions. A high-quality, wafer-scale h-BN film is confirmed by various characterizations. Dielectric property of as-grown h-BN film is evaluated by characterization of Co(foil)/h-BN/Co(contact) capacitor devices. Breakdown electric field is in the range of 3.0-3.3 MV/cm, which indicates that the epitaxial h-BN film has good insulating characteristics. In addition, the effect of substrate morphology on h-BN growth is discussed regarding different domain density, lateral size, and thickness of the h-BN films grown on unpolished and polished Co foils.

In summary, we have developed and optimized MBE based growth of multilayer h-BN, single/multi-layer graphene, as well as their vertical and in-plane heterostructures. Structural, electrical and optical characterization has been carried out to evaluate electrical and optical properties of the films. Our results reveal that MBE, as a versatile tool, can provide an excellent alternative way for reliable growth of high-quality and

large-size 2D materials and their heterostructures, which will attract more attention for the utilization of MBE in 2D materials research.

Appendix

Publications:

1) Z. Zuo, Z. Xu (co-first author), R. Zheng, A. Khanaki, J. Zheng, and J. Liu, Sci. Rep., 5, 14760 (2015)".

http://www.nature.com/articles/srep14760.

2) Z. Xu, R. Zheng, A. Khanaki, Z. Zuo, and J. Liu, Appl. Phys. Lett. 207, 213103(2015)".

http://scitation.aip.org/content/aip/journal/apl/107/21/10.1063/1.4936378.

3) Z. Xu, A. Khanaki, H. Tian, R. Zheng, M. Suja, J. Zheng and J. Liu, Appl. Phys. Lett. 109,043110 (2016).

http://scitation.aip.org/content/aip/journal/apl/109/4/10.1063/1.4960165.

4) Z. Xu, H. Tian, A. Khanaki, R. Zheng, M. Suja, and J. Liu, submitted to Scientific Report on August 5th (2016) .